1 **The imprinted *Zdbf2* gene finely tunes feeding and growth in neonates**

2

3

4

5

6

7 Juliane Glaser[1,4], Julian Iranzo[1], Maud Borensztein[1], Mattia Marinucci[1], Angelica Gualtieri[3],

8 Colin Jouhanneau[2], Aurelie Teissandier[1], Carles Gaston-Massuet[3], and Deborah Bourc'his[1][*]

9

10

11

12   1. Institut Curie, PSL Research University, INSERM, CNRS, Paris 75005, France

13   2. Institut Curie, PSL Research University, Animal Transgenesis Platform, Paris 75005,

14   France

15   3. Centre for Endocrinology, William Harvey Research Institute, Barts and the London

16   School of Medicine and Dentistry, Queen Mary University of London, London EC1M

17   6BQ, UK.

18   4. Present address: RG Development & Disease, Max Planck Institute for Molecular

19   Genetics, Berlin, Germany

20

21

22

23 * Correspondence: **deborah.bourchis@curie.fr**

24

1

25   **ABSTRACT**

26

27   Genomic imprinting refers to the mono-allelic and parent-specific expression of a subset of

28   genes. While long recognized for their role in embryonic development, imprinted genes have

29   recently emerged as important modulators of postnatal physiology, notably through

30   hypothalamus-driven functions. Here, using mouse models of loss, gain and parental inversion

31   of expression, we report that the paternally expressed *Zdbf2* gene controls neonatal growth in

32   mice, in a dose-sensitive but parent-of-origin-independent manner. We further found that

33   *Zdbf2*-KO neonates failed to fully activate hypothalamic circuits that stimulate appetite, and

34   suffered milk deprivation and diminished circulating Insulin Growth Factor 1 (IGF-

35   1). Consequently, only half of *Zdbf2*-KO pups survived the first days after birth and those

36   surviving were smaller. This study demonstrates that precise imprinted gene dosage is

37   essential for vital physiological functions at the transition from intra- to extra-uterine life, here

38   the adaptation to oral feeding and optimized body weight gain.

39

40   **Keywords:** Genomic imprinting/ Development/ Growth/ Hypothalamus

INTRODUCTION

Genomic imprinting is the process by which a subset of genes is expressed from only one copy in a manner determined by the parental origin. In mammals, genomic imprinting arises from sex-specific patterning of DNA methylation during gametogenesis, which generates thousands of germline differentially methylated regions (gDMRs) between the oocyte and the spermatozoa. After fertilization, the vast majority of gDMRs are lost during the epigenetic reprogramming that the embryonic genome undergoes (Seah & Messerschmidt, 2017). However, some gDMRs are protected through sequence- and DNA methylation-specific recruitment of the KRAB-associated protein 1 (KAP1) complex (Li *et al*, 2008; Quenneville *et al*, 2011; Takahashi *et al*, 2019) and become fixed as imprinting control regions (ICRs). Roughly 20 ICRs maintain parent-specific DNA methylation throughout life and across all tissues in mouse and human genomes, and control the mono-allelic and parent-of-origin expression of approximately 150 imprinted genes (Schulz *et al*, 2008; Tucci *et al*, 2019).

DNA methylation-based genome-wide screens have led to the conclusion that all life-long ICRs have probably been discovered (Proudhon *et al*, 2012; Xie *et al*, 2012). However, a greater number of regions are subject to less robust forms of imprinted DNA methylation, restricted to early development or persisting in specific cell lineages only. Moreover, imprinted genes are often expressed in a tissue- or stage-specific manner (Proudhon *et al*, 2012; Monteagudo-Sánchez *et al*, 2019), adding to the spatio-temporal complexity of genomic imprinting regulation. Finally, while the vast majority of imprinted genes are conserved between mice and humans, a subset of them have acquired imprinting more recently in a species-specific manner (Bogutz *et al*, 2019). Why is reducing gene dosage important for imprinted genes, why does it occur in a parent-of-origin manner and why is it essential for specific organs in specific species are fundamental questions in mammalian development and physiology.

Imprinted genes have long-recognized roles in development and viability *in utero*, by balancing growth and resource exchanges between the placenta and the fetus. Moreover, it is increasingly clear that imprinted genes also strongly influence postnatal physiology (Peters, 2014). Neonatal growth, feeding behavior, metabolic rate and body temperature are affected by improper dosage of imprinted genes in mouse models and human imprinting disorders (Charalambous *et al*, 2014; Ferrón *et al*, 2011; Leighton *et al*, 1995; Li *et al*, 1999; Plagge *et al*, 2004; Nicholls *et al*, 1989; Buiting, 2010). Imprinting-related postnatal effects are recurrently linked to dysfunction of the hypothalamus (Ivanova & Kelsey, 2011), a key organ for orchestrating whole body homeostasis through a complex network of nuclei that produce and deliver neuropeptides to distinct targets, including the pituitary gland that in turn secretes endocrine hormones such as the growth hormone (GH). Accordingly, the hypothalamus

76   appears as a privileged site for imprinted gene expression (Gregg *et al*, 2010). A typical

77   illustration of such association is provided by a cluster of hypothalamic genes whose dosage

78   is altered in Prader-Willi syndrome (PWS). PWS children present neurological and behavioral

79   impairments in particular related to feeding, in the context of hypothalamic neuron anomalies

80   (Swaab, 1997; Cassidy & Driscoll, 2009). In mouse models, single inactivation of the PWS-

81   associated *Magel2* gene results in neonatal growth retardation, reduced food intake and

82   altered metabolism (Bischof *et al*, 2007; Kozlov *et al*, 2007; Schaller *et al*, 2010). Fine-tuning

83   hypothalamic inputs is particularly important for adapting to environmental changes, the most

84   dramatic one for mammals being the transition from intra- to extra-uterine life at birth. Early

85   mis-adaptation to postnatal life can have far-reaching consequences on adult health, by

86   increasing the risk of metabolic diseases. It therefore is of the outmost importance to

87   thoroughly document the action of imprinted genes, particularly in hypothalamic functions.

88   *Zdbf2* (*DBF-type zinc finger- containing protein 2*) is a paternally expressed gene with

89   preferential expression in the brain (Kobayashi *et al*, 2009; Greenberg *et al*, 2017). It is one of

90   the last-discovered genes with life-long and tissue-wide imprinted methylation, and conserved

91   imprinting in mice and humans, however its function is not yet resolved (Kobayashi *et al*, 2009;

92   Duffié *et al*, 2014). We previously characterized the complex parental regulation of the *Zdbf2*

93   locus: it is controlled by a maternally methylated gDMR during the first week of embryogenesis,

94   but for the rest of life, it harbors a somatic DMR (sDMR) that is paternally methylated

95   (Proudhon *et al*, 2012; Duffié *et al*, 2014) (Figure1A). The maternal gDMR coincides with a

96   promoter that drives paternal-specific expression of a *Long isoform of Zdbf2* (*Liz*) transcript. In

97   the pluripotent embryo, *Liz* transcription triggers *in cis* DNA methylation at the sDMR, allowing

98   de-repression of the canonical promoter of *Zdbf2*, located ~10kb downstream (Greenberg *et*

99   *al*, 2017) (Figure1A). In fact, although specifically expressed in the embryo where it undergoes

100   stringent multi-layered transcriptional control (Greenberg *et al*, 2019), *Liz* is dispensable for

101   embryogenesis itself. Its sole function seems to epigenetically program expression of *Zdbf2*

102   later in life: genetic loss-of-function of *Liz* (*Liz*-LOF) prevents methylation of the sDMR, giving

103   rise to mice that cannot activate *Zdbf2* –despite an intact genetic sequence– in the

104   hypothalamus and the pituitary gland and display reduced postnatal growth (Greenberg *et al*,

105   2017). The cause of this growth phenotype and whether it is directly linked to the function and

106   dosage regulation of *Zdbf2* in the brain cells is unknown.

107   By generating loss-of-function (LOF) and gain-of-function (GOF) mouse mutants, we

108   show here that ZDBF2 is necessary for optimal growth and survival during the nursing period,

109   by stimulating hypothalamic food circuits immediately at birth. Moreover, our data support that

110   the dose but not the parental origin of *Zdbf2* expression is important for its imprinted mode of

111   action. Altogether, our study illustrates the critical function and proper dose regulation of *Zdbf2*

112   for adaptation to postnatal life.

113   **RESULTS**
114

115   ***Zdbf2* is expressed in the neuro-endocrine cells of the hypothalamo-pituitary axis.**

116   Besides a C2H2 zinc finger motif, the ZDBF2 protein does not contain any obvious functional
117   domain that could inform its molecular function. To gain insights into the role of *Zdbf2*, we first
118   examined the cellular specificity and temporal dynamics of its expression. Comprehensive
119   datasets of adult tissues expression in mice and human suggested *Zdbf2* expression is
120   prevalent in brain tissues and pituitary gland (biogps in mouse tissues:
121   http://biogps.org/#goto=genereport&id=73884 and GTex in human tissues:
122   https://gtexportal.org/home/gene/ZDBF2). Our data endorse this brain and pituitary-specific
123   expression of *Zdbf2* in adult mice and show the highest level of expression in the hypothalamus
124   (Figure S1A) (Greenberg *et al*, 2017).

125   To resolve the cellular specificity of *Zdbf2* expression, we used a previously described
126   *LacZ* reporter *Zdbf2* gene-trap mouse line (Greenberg *et al*, 2017). X-gal staining of 2 week-
127   old brain sections confirmed the expression of *Zdbf2* in various brain tissues and the high
128   specificity in hypothalamic cells that belonged to the peri- and paraventricular nuclei in the
129   anterior area (Figure 1B), and the arcuate, the dorsomedial and the ventromedial nuclei in the
130   lateral hypothalamic area (Figure 1C). Analysis of publicly available single-cell RNA-
131   sequencing (scRNA-seq) data further defined *Zdbf2* expression to be specific to neuronal cells
132   and absent from non-neuronal cells of the hypothalamus (Figure S1B-C) (Chen et al., 2017).
133   The three hypothalamic clusters where *Zdbf2* was the most highly expressed were both
134   glutamatergic (Glu13 and Glu15) and GABAergic (GABA17) neurons from the arcuate and the
135   periventricular hypothalamic regions (Figure S1B). Interestingly, these nuclei synthesize
136   peptides that stimulate hormone production from the pituitary gland, or that control energy
137   balance –food intake, energy expenditure and body temperature– by directly acting on the
138   brain and/or more distal organs (Saper & Lowell, 2014).

139   *Zdbf2* being also expressed in the pituitary gland (Figure S1A), we hypothesized it
140   could have a role in the hypothalamo-pituitary axis. When we exanimated the pituitary gland
141   by X-gal staining, we found *Zdbf2* to be expressed in the anterior and intermediate lobes of
142   the gland and almost undetectable signal in the posterior lobe (Figures 1D and S1D), a pattern
143   that was confirmed from available scRNA-seq data (Figure S1E) (Cheung et al., 2018). The
144   anterior and intermediate lobes that form the adenohypophysis are responsible for hormone
145   production (Mollard *et al*, 2012). The anterior lobe secretes hormones from five different
146   specialized hormone-producing cells under the control of hypothalamic inputs (growth
147   hormone-GH, adrenocorticotropic hormone-ACTH, thyroid stimulating hormone-TSH,
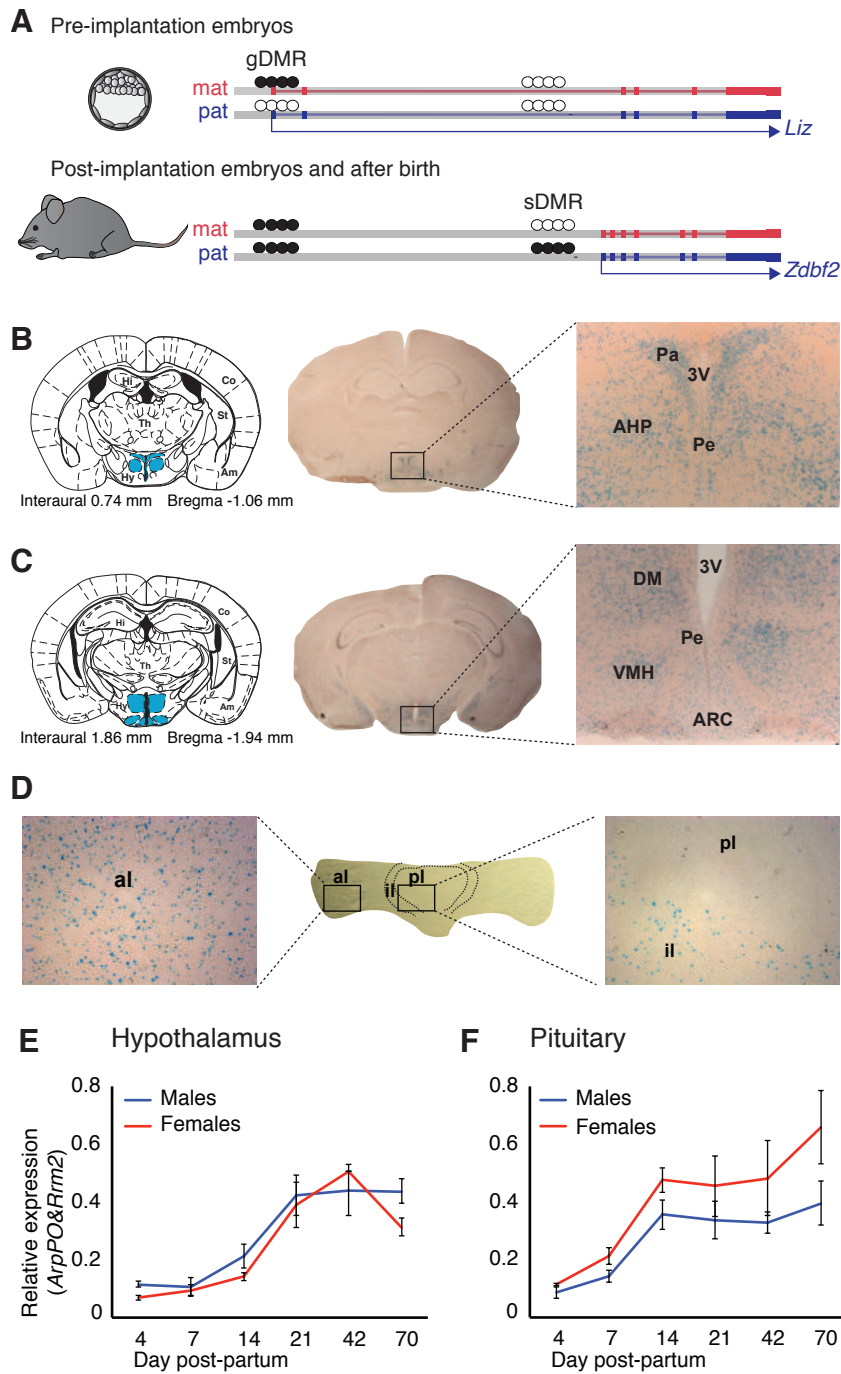
6

Glaser et al._ Figure 1

Figure 1: *Zdbf2* expression localizes preferentially in the neuro-endocrine cells of the hypothalamo-pituitary axis in juvenile animals.

(**A**) Scheme of the *Liz/Zdbf2* locus regulation during mouse development. In the pre-implantation embryos, a maternally methylated gDMR allow the paternal-specific expression of the Long isoform of *Zdbf2* (*Liz*). *Liz* expression triggers, in cis, DNA methylation at the sDMR which is localized 8kb upstream of *Zdbf2* canonical promoter. In the post-implantation embryos and for the rest of the life, the imprint at the locus is controlled by the paternal methylation at the sDMR and this allow de-repression of *Zdbf2*, leading to its paternal-specific expression in the post-natal brain. (**B, C**) X-gal staining on brain coronal sections from 2-week-old *Zdbf2*-lacZ transgenic males. The coronal diagram from the Mouse Brain Atlas (left panel) localizes the sections in zone 40 (**B**) and zone 47 (**C**) in stereotaxic coordinates, with the hypothalamus indicated in blue. Whole brain coronal sections (middle panel) show specific staining in the hypothalamus, due to several positive hypothalamic nuclei (right panel, 20X magnificence). Hi, hippocampus; Co, cortex; Th, thalamus; Am, amygdala; St, striatum; Hy, hypothalamus; 3V, third ventricule; Pa, paraventricular hypothalamic nucleus; Pe, periventricular hypothalamic nucleus; AH, anterior hypothalamic area; DM, dorsomedial hypothalamic nucleus; VMH, ventromedial hypothalamic nucleus; Arc, arcuate hypothalamic nucleus. (**D**) X-gal staining on pituitary horizontal sections. The posterior lobe of the pituitary shows no X-gal staining (right panel), while staining is evenly distributed in the anterior lobe (left panel). pl, posterior lobe; il, intermediate lobe; al, anterior lobe. (**E, F**) *Zdbf2* expression measured by RT-qPCR in the hypothalamus (**E**) and the pituitary (**F**) from 4 to 70 days after birth. Data are shown as mean ± s.e.m. of n=3 C57Bl6/J mice.

7

149   luteinizing hormone-LH and prolactin-PRL) and the intermediate lobe contains

150   melanotrope cells (Kelberman *et al*, 2009). Altogether, the expression specificity of *Zdbf2*

151   suggests a role in functions of the endocrine hypothalamo-pituitary axis and/or of the

152   hypothalamus alone. Finally, we further found that steady-state levels of *Zdbf2* transcripts

153   progressively rose in the hypothalamus and the pituitary gland after birth, reached their

154   maximum at 2-3 weeks and then stabilized at later ages, in both males and females (Figures

155   1E and 1F). The expression of *Zdbf2* therefore mostly increases in juvenile pups prior to

156   weaning.

157

ZDBF2 positively regulates growth postnatally.

159   In *Liz*-LOF mutants, *Zdbf2* failed to be activated and animals displayed postnatal body weight

160   reduction (Greenberg *et al*, 2017). However, whether this was directly and only linked to *Zdbf2*

161   deficiency was not resolved. To directly probe the biological role of ZDBF2, we therefore

162   generated a mouse model of a genetic loss-of function of *Zdbf2*. More specifically, we

163   engineered a ~700bp deletion of the entirety of exon 6 (Figure 2A) that is common to all

164   annotated *Zdbf2* transcripts (Duffié *et al*, 2014). The *Zdbf2*-Δexon6 deletion induces a frame-

165   shift predicted to generate a severely truncated protein (wild-type 2494aa versus 19aa mutant

166   protein) that notably lacks the zinc finger motif. As *Zdbf2* is an imprinted gene with paternal-

167   specific expression, the deletion should exhibit an effect upon paternal but not maternal

168   transmission. For simplicity, heterozygous mutants with a paternally inherited *Zdbf2*-Δexon6

169   deletion are thus referred to as *Zdbf2*-KO thereafter.

170   At birth, we found that *Zdbf2*-KO animals were present at expected sex and Mendelian

171   ratios (Figures S2A and S2B). However, while exhibiting normal weight prior to birth (at

172   embryonic day E18.5), *Zdbf2*-KO neonates of both sexes failed to thrive from the first day of

173   postnatal life (day post-partum, dpp) (Figure 2B-D). Growth reduction was the most drastic

174   prior to weaning, from 5 to 21dpp (Figure 2B): at 2 weeks of age, *Zdbf2*-KO mice were 20%

175   lighter than their WT littermates (Figures 2B, 2E and 2F). Body weight reduction persisted

176   through adulthood, with a tendency to minimize with age (Figure 2B). As predicted, when

177   present on the maternal allele, the *Zdbf2*-Δexon 6 deletion had no discernable growth effect

178   (Figures S2C and S2D).

179   The reduced body weight phenotype was fully penetrant (Figure S2E) and was not due

180   to a developmental delay: *Zdbf2*-KO pups and their WT littermates synchronously acquired

181   typical hallmarks of postnatal development (skin pigmentation, hair appearance and eye

182   opening) (Figure S2F-I). The growth phenotype appeared to be systemic: it affected both the

183 length and the weight of *Zdbf2*-KO animals (Figure S3A) and all organs uniformly (Figure S3B),

184 such that body proportion was maintained. To gain insight into the origin of the body weight

185 restriction, we performed dual-energy X-ray absorptiometry (DEXA) scan at 7 weeks of age to

186 measure *in vivo* the volume fraction of the three dominant contributors to body composition:

187 adipose, lean, and skeletal tissues (Chen et al., 2012). While we confirmed that adult *Zdbf2*-

188 KO males exhibit an overall body weight reduction (Figure S3C), we did not observe difference

189 in the composition of fat and bone tissues (Figures 2G and S3D-F). However, *Zdbf2*-KO mice

190 had decreased lean mass (Figure 2H). Collectively, the above analyses demonstrate that the

191 product of *Zdbf2* positively regulates body weight gain in juvenile mice.

192 In conclusion, *Zdbf2*-KO animals exhibit the same growth defect that we previously

193 reported in *Liz*-LOF mice, with identical postnatal onset and severity (Greenberg *et al*, 2017).

194 However, contrary to the *Liz*-LOF mice, the regulatory landscape of the paternal allele of *Zdbf2*

195 was intact in *Zdbf2*-KO mice: DNA methylation of the sDMR located upstream of *Zdbf2* was

196 normal (Figure S3G), and accordingly, *Zdbf2* transcription was activated (Figure S3H). This

197 supports that *Liz* transcription in the early embryo —which is required for sDMR DNA

198 methylation (Greenberg *et al*, 2017)— is not impacted in the *Zdbf2*-KO model. We therefore

199 show that a genetic mutation of *Zdbf2* (*Zdbf2*-KO) and a failure to epigenetically program *Zdbf2*

200 expression (*Liz*-LOF) are phenotypically indistinguishable. As *Liz*-LOF mice show a complete

201 lack of *Zdbf2* expression (Greenberg *et al*, 2017), this incidentally supports that *Zdbf2*-KO mice

202 carry a null *Zdbf2* allele. Unfortunately, we failed to specifically detect the mouse ZDBF2

203 protein with commercial or custom-made antibodies.

204

205 **Zdbf2-KO neonates fail to thrive or die prematurely within the first week of age.**

206 Growth restriction during the nursing period could dramatically impact the viability of *Zdbf2*-KO

207 pups. Indeed, analysis of *Zdbf2*-KO cohorts revealed that although there was no Mendelian

208 bias at 1dpp (Figure S2B), a strong bias was apparent at 20dpp: 75 WT and 44 *Zdbf2*-KO

209 animals were weaned among *n*=27 litters, while a 50/50 ratio was expected. Post-natal

210 survivability was the most strongly impaired within the first days after birth, with only 56% of

211 *Zdbf2*-KO males and 52% of *Zdbf2*-KO females still alive at 3dpp, compared to 84 and 88% of

212 WT survival at this age (Figure 2I and Supplemental Table 1A). Importantly, a partial postnatal

213 lethality phenotype was also present in *Liz*-LOF mutants who are equally growth-restricted as

214 a result of *Zdbf2* deficiency (Figure S3I), but did not occur when the mutation was transmitted

215 from the silent maternal allele harboring either the *Zdbf2* deletion or the *Liz* deletion (Figure

216 S3J and S3K and Supplemental Table 1C).
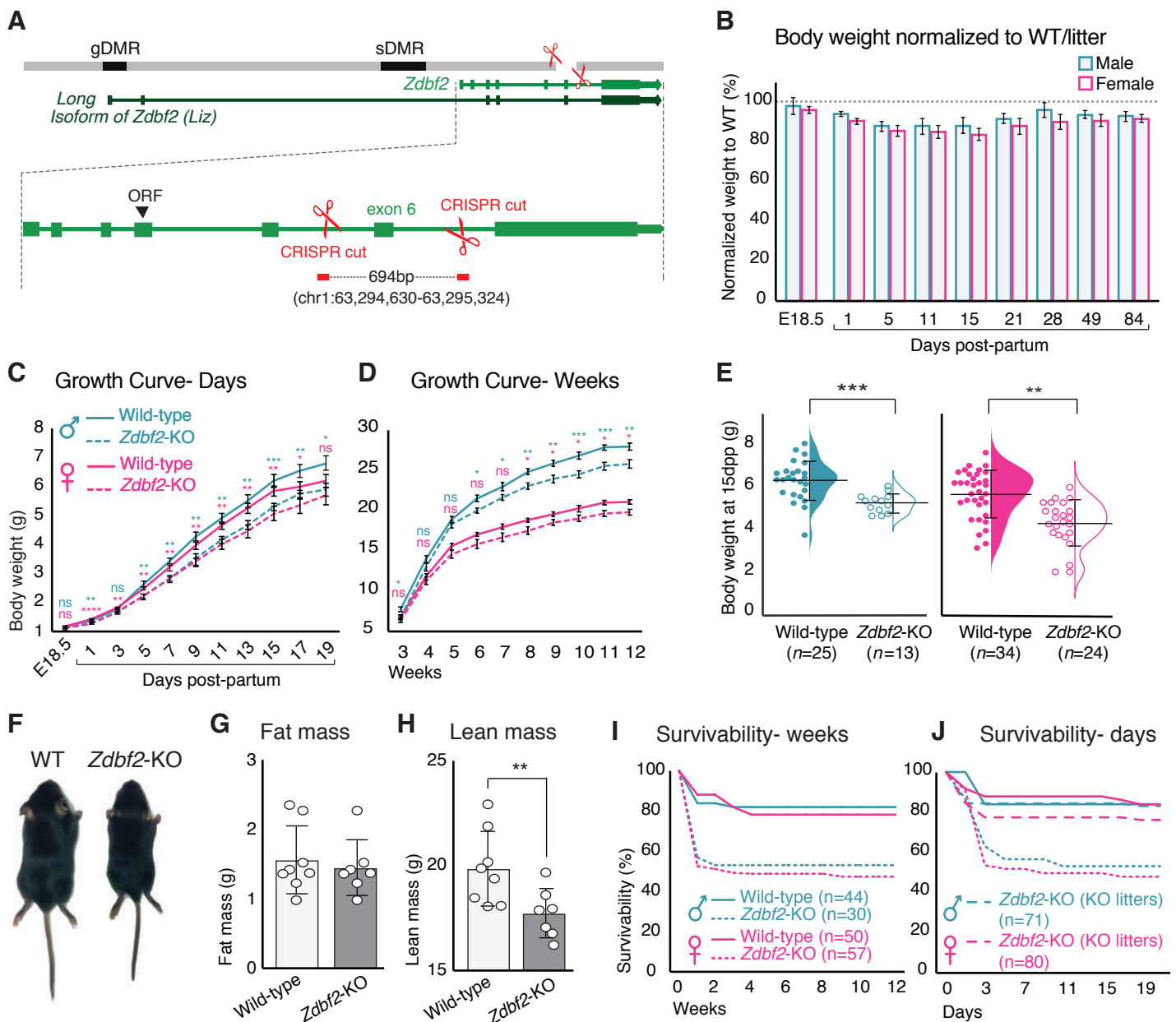
Glaser et al._ Figure 2

Figure 2: *Zdbf2*-KO mice exhibit growth reduction and partial post-natal lethality.
(**A**) Graphical model of the *Zdbf2* deletion generated using two sgRNAs across exon 6. The two differentially methylated (DMR) regions of the locus are indicated (germline-gDMR, and somatic-sDMR), as well as the Long Isoform of *Zdbf2* (*Liz*). The ORF(Open Reading Frame) of *Zdbf2* starts in exon 4. Genomic coordinates of the deletion are indicated. (**B**) Body weight of *Zdbf2*-KO mice normalized to WT littermates (100%) followed from embryonic day E18.5 to 84 days post-partum. Data are shown as means ± s.e.m. from individuals from n= 27 litters. (**C, D**) Growth curve comparing the body weights of WT and *Zdbf2*-KO mice prior to weaning, from E18.5 to 19dpp (**C**) and over 3 months after birth (**D**). n=15–50 mice were analyzed per genotype, depending on age and sex. Statistical analyses were performed by a two-tailed, unpaired, nonparametric Mann Whitney t test. ***p ≤ 0.001,**p ≤ 0.01, *p≤ 0.05. (**E**) Half dot plot- half violin plot showing the weight distribution in 2 week-old males (left) and females (right) of WT and *Zdbf2*-KO genotypes. Statistical analyses were performed by a two-tailed, unpaired, nonparametric Mann Whitney t test. ***p ≤ 0.001,**p ≤ 0.01, *p≤ 0.05. (**F**) Representative photography of a smaller 2 week-old *Zdbf2*-KO male compared to a WT littermate. (**G-H**) Dual-energy X-ray absorptiometry (DXA) analysis showing the calculation of fat mass (**G**) and lean mass (**H**) in WT and *Zdbf2*-KO males at 7 weeks. Data are shown as means ± s.e.m. from n= 8 WT and n=7 *Zdbf2*-KO males. (**I**) Kaplan-Meier curves of the survivability from birth to 12 weeks of age comparing WT (plain lines) and *Zdbf2*-KO (dotted lines) littermates from WT x *Zdbf2* KO/WT backcrosses. Impaired survivability occurs specifically from the first day to 2 weeks of age. (**J**) Kaplan-Meier curves of the survivability from 1 to 21dpp comparing *Zdbf2*-KO pups generated from WT x *Zdbf2* KO/KO intercrosses, with *Zdbf2*-KO and their WT littermates generated from WT x *Zdbf2* KO/WT backcrosses. *Zdbf2*-KO pups are more prone to die only when they are in competition with WT littermates (small dotted lines), while *Zdbf2*-KO pups have a normal survivability when they are not with WT littermates (large dotted lines).

218   To determine whether partial lethality was due to a vital function of ZDBF2, *per se,* or to a
219   competition with WT littermates, we monitored survivability in litters of only *Zdbf2*-KO pups
220   generated from crosses between WT females x homozygous *Zdbf2*-KO/KO males. Litter sizes
221   were similar than the ones sired by *Zdbf2*-KO/WT males. However, when placed in an
222   environment without WT littermates, *Zdbf2*-KO pups gained normal survivability (Figure 2J and
223   Supplemental Table 1B). Incidentally, this shows that *Zdbf2*-KO pups have the mechanical
224   ability to suckle milk. More likely, the impaired survival of *Zdbf2*-KO neonates is a consequence
225   of intra-litter competition with healthier WT pups. Overall, our detailed study of the *Zdbf2*-KO
226   phenotype reveals that smaller *Zdbf2*-KO neonates have reduced fitness compared to their
227   WT littermates. In absence of ZDBF2, after a week of life, half of juvenile pups did not survive
228   and the other half failed to thrive.

229

230   **Postnatal body weight control is highly sensitive to *Zdbf2* dosage**

231   The physiological effects of imprinted genes are intrinsically sensitive to both decreases and
232   increases in the expression of imprinted genes. We therefore went on assessing how postnatal
233   body weight gain responded to varying doses of the imprinted *Zdbf2* gene. We first analyzed
234   the growth phenotype resulting from partial reduction in *Zdbf2* dosage, as compared to a total
235   loss of *Zdbf2* in *Zdbf2*-KO mice. For this, we used the *LacZ* reporter *Zdbf2* gene-trap mouse
236   line (Greenberg *et al*, 2017), in which the insertion of the *LacZ* cassette downstream of exon
237   5 does not fully abrogate the production of full-length *Zdbf2* transcripts (Figure S4A). Upon
238   paternal inheritance of this allele, animals still express 50% of WT full-length *Zdbf2* mRNA
239   levels in the hypothalamus and the pituitary gland (Figure S4B and S4C). Interestingly, these
240   mice displayed significant weight reduction compared to their WT littermates (Figure S4D), but
241   less severe than *Zdbf2*-KO mice (Figure 2B-D). On average, we observed a 5 to 10% weight
242   reduction from 7 to 21dpp, which is incidentally half the growth reduction observed in *Zdbf2*-
243   KO mice for the same age range.

244   We then assessed the consequences of increased *Zdbf2* dosage, with the hypothesis
245   that this would lead to excessive body weight gain after birth, as opposed to reduced *Zdbf2*.
246   For this, we took advantage of a *Zdbf2* gain-of-function (GOF) line that we serendipitously
247   obtained when generating *Liz* mutant mice (Greenberg *et al*, 2017) (see detailed description
248   in Supplemental information). The *Zdbf2*-GOF lines carry a ~ 900bp deletion upstream of *Liz*
249   exon 1, which leaves some part of exon 1 intact and induces an epigenetic "paternalization" of
250   the maternal allele of the locus (Figure S4E and S4F). While sDMR methylation and *Zdbf2*
251   activation exclusively occur on the paternal allele during normal development, animals that
252   maternally inherit this partial deletion also acquire sDMR methylation on the maternal allele

11

253   (Figures 3A and S4F-H) and activate *Zdbf2* from the maternal allele, although slightly less than

254   from the WT paternal allele (Figure 3B). As a consequence, *Zdbf2*-GOF animals exhibit bi-

255   allelic *Zdbf2* expression, with a net 1.7-fold increase of *Zdbf2* levels in postnatal hypothalamus

256   and pituitary gland, as compared to WT littermates that express *Zdbf2* mono-allelically, from

257   the paternal allele only (Figure 3C).

258   Importantly, we found that increased *Zdbf2* dosage was indeed impactful for postnatal

259   body weight: *Zdbf2*-GOF animals were consistently overweight (Figure 3D-F), and their

260   viability was normal (Figure S5A-C). Although *Zdbf2* was overexpressed in both *Zdbf2*-GOF

261   males and females, the overgrowth phenotype was male-specific, which may imply stimulation

262   of the phenotype by sex hormones, directly or indirectly. Similar to growth restriction observed

263   in *Zdbf2*-KO mutant mice, increased body weight of *Zdbf2*-GOF males was more pronounced

264   during the nursing period (Figure 3D, G and H) and affected all organs uniformly (Figure S5D).

265   From 10 to 20dpp, *Zdbf2*-GOF juvenile males were 10% heavier when normalized to the

266   average WT siblings from the same litter (Figure 3D). At 2 weeks of age, *Zdbf2*-GOF males

267   were visibly bigger than their WT littermates (Figure 3G and 3H), while females displayed

268   standard normal distribution (Figure S5E). Comparatively, progenies from a paternal

269   transmission of the deletion showed a growth progression similar to their WT littermates

270   (Figure S5F and S5G). Overall, these data illustrate the importance of *Zdbf2* for the regulation

271   of postnatal body weight gain at the onset of postnatal life. We therefore demonstrate that the

272   *Zdbf2* imprinted gene encodes a genuine positive regulator of postnatal body weight gain in

273   mice, with highly attuned dose-sensitive effects.

274

275   **_Zdbf2_ regulates post-natal growth in a parent-of-origin independent manner.**

276   Imprinted genes with a paternal expression generally tend to enhance prenatal and postnatal

277   growth (Haig, 2000). Consistently, we found that the paternally expressed *Zdbf2* gene

278   promotes postnatal weight gain. Having determined the dosage effect of *Zdbf2*, we next

279   wondered what role plays the paternal origin of *Zdbf2* expression on postnatal body weight.

280   To invert *Zdbf2* parental expression, we intercrossed the *Liz*-LOF and *Zdbf2*-GOF lines, which

281   consist in a maternalization of the paternal allele and a paternalization of the maternal allele of

282   *Zdbf2*, respectively. By crossing an heterozygous *Zdbf2*-GOF female with an heterozygous

283   *Liz*-LOF male (Figure 4A, left panel), four genotypes can segregate in the progeny, with

284   littermates displaying various dosage and parent-of-origin expression of *Zdbf2* (Figure 4A): *1)*

285   wild-type animals with one dose of paternal *Zdbf2* expression, *2)* animals with a paternal *Liz*-

286   LOF allele and lack of *Zdbf2* expression (equivalent to a *Zdbf2*-loss-of-function, *Zdbf2*-LOF),

287   *3)* animals with a maternal *Zdbf2*-GOF allele and biallelic *Zdbf2* expression, and finally, *4)*
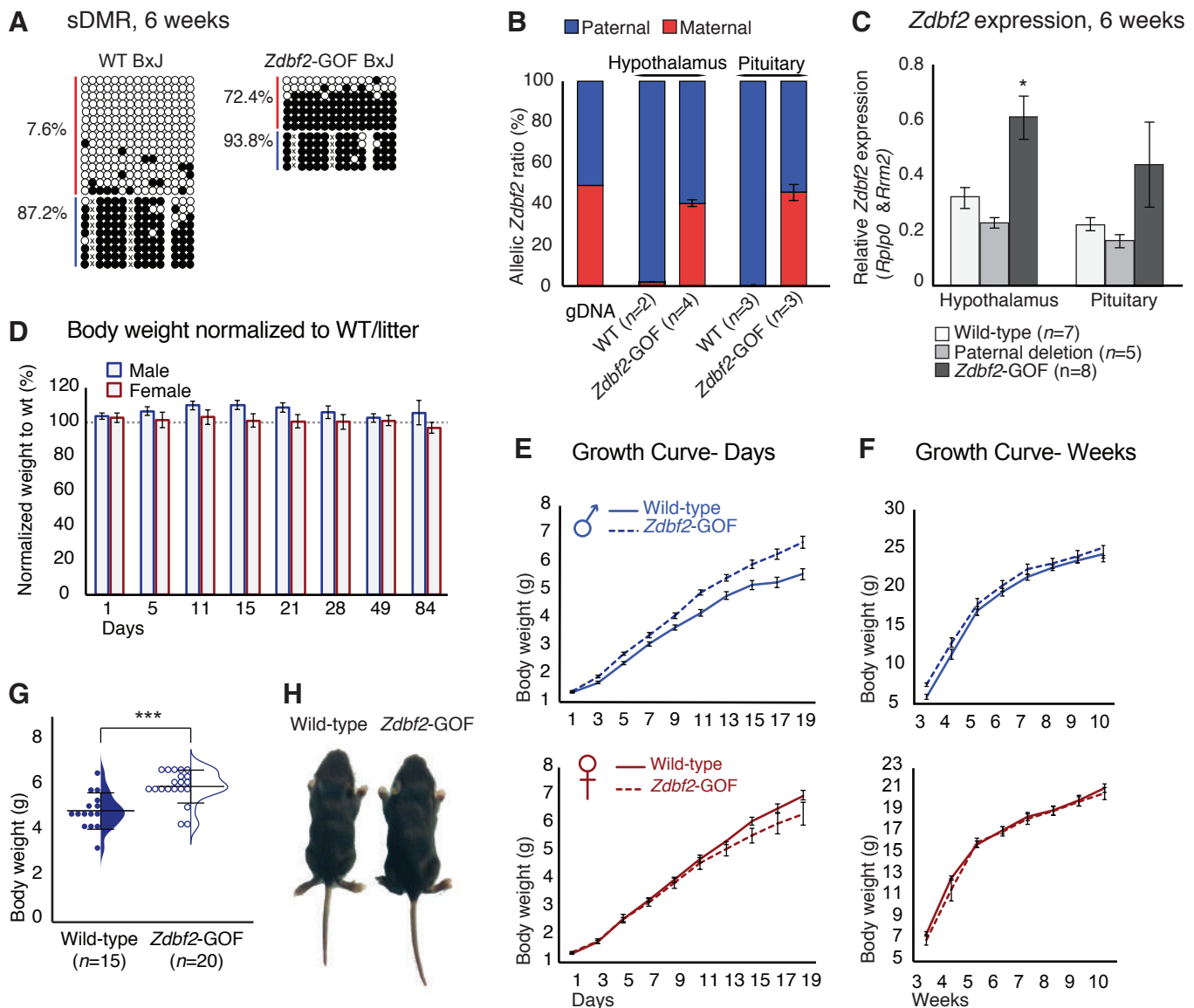
12

Glaser et al._ Figure 3

Figure 3: *Zdbf2* influences postnatal growth in a dose-dependent manner.
(**A**) Bisulfite cloning and sequencing showing CpG methylation levels at the sDMR locus of hypothalamus DNA from 6-week-old hybrid WT (left) and *Zdbf2*-GOF (right) mice (*Zdbf2*-GOF +/- x JF1 cross). Red, maternal alleles; blue, paternal alleles. cross, informative JF1 SNP. (**B**) Allelic expression of *Zdbf2* in hypothalamus and pituitary gland from 3-week-old mice, measured by RT-pyrosequencing. Genomic DNA extracted from a C57Bl/6 x JF1 hybrid cross was used as a control for pyrosequencing bias. (**C**) RT-qPCR measurement reveals a ~ 1.7 fold-increase of *Zdbf2* expression in the hypothalamus and pituitary gland of 3 week-old mice with a maternal transmission of the deletion. Expression of *Zdbf2* in mice carrying the deletion on the paternal allele is similar to WT. (**D**) Normalized body growth of *Zdbf2*-GOF mice to their WT littermates (100%) followed at different ages (1 to 84 days) from n=14 litters. The overgrowth is seen specifically in males, from 5 to 28 days. (**E, F**) Growth curves of female and male mice, comparing the body weights of WT and *Zdbf2*-GOF, through the 3 first weeks of life (D) and through 10 weeks (E). n=10–30 mice were analyzed per genotype, depending on age and sex. (**G**) Half dot- half violin plots showing the weight distribution at 2 weeks of age between WT and *Zdbf2*-GOF males. Data are shown as means ± s.e.m. from n individuals. Statistical analyses were performed by a two-tailed, unpaired, nonparametric Mann Whitney t test. *** p ≤ 0.005. (**H**) Representative photography of a bigger *Zdbf2*-GOF male as compared to a WT littermate at 2 weeks.

13

289 animals with combined maternal *Zdbf2*-GOF and paternal *Zdbf2*-LOF alleles and potentially,

290 mono-allelic, reverted maternal expression of *Zdbf2* (Figure 4A, right panel).

291   The uniform strain background of the two lines did not allow us to use strain-specific

292 sequence polymorphisms to distinguish the parental origin of *Zdbf2* regulation in the compound

293 *Zdbf2*-GOF/*Zdbf2*-LOF animals. However, we found that compared to single *Zdbf2*-LOF

294 mutants, the presence of the maternal *Zdbf2*-GOF allele restored DNA methylation levels at

295 the sDMR locus in all tissues of *Zdbf2*-GOF/*Zdbf2*-LOF mutants, with an average of 43.5%

296 CpG methylation compared to the expected 50% in WT (Duffié *et al*, 2014) (Figure S5H). By

297 RT-qPCR, *Zdbf2* mRNA levels were also increased in the hypothalamus and pituitary gland of

298 *Zdbf2*-GOF/*Zdbf2*-LOF animals compared to single *Zdbf2*-LOF animals (Figure 4B), which

299 strongly suggests that expression comes from the maternal *Zdbf2*-GOF allele. Accordingly,

300 *Zdbf2* expression level in *Zdbf2*-GOF/*Zdbf2*-LOF animals was on average 0.65-fold the one of

301 WT animals, which is congruent with the partial paternalization of the maternal *Zdbf2*-GOF

302 allele we reported (Figures 4B and S4I). Most importantly, restoration of *Zdbf2* expression by

303 the maternal *Zdbf2*-GOF allele -even though incomplete- was sufficient to rescue the postnatal

304 body weight phenotype in compound *Zdbf2*-GOF/*Zdbf2*-LOF males compared to their single

305 *Zdbf2*-LOF brothers (Figure 4C and 4D). From a body weight reduction of 20% reported in *Liz*-

306 LOF or *Zdbf2*-KO animals at the same age, it was attenuated to only 4% in *Zdbf2*-GOF/*Zdbf2*-

307 LOF animals (Figure 4C), showing that maternal *Zdbf2* expression is as functional as paternal

308 *Zdbf2* expression. Altogether, these results crystallize the importance of *Zdbf2* dosage in

309 regulating postnatal body weight and most importantly, demonstrate that the dose but not the

310 parental origin matters for *Zdbf2* function.

311

312 **_Zdbf2_-KO growth phenotype is linked to decreased IGF-1 in the context of normal**

313 **development of the hypothalamo-pituitary axis.**

314 Having demonstrated the growth promoting effect of *Zdbf2*, we next tackle the question of how

315 it influences newborns weight and survival. As *Zdbf2* is expressed in the neuroendocrine cells

316 of the hypothalamo-pituitary axis, the phenotype of *Zdbf2*-KO animals may lay in a defect in

317 producing growth-stimulating pituitary hormones. When we assessed the development and

318 functionality of the hypothalamus and pituitary gland prior to birth, we did not detect any

319 morphological nor histological defects in *Zdbf2*-KO embryos (Figure S6A-C). Normal

320 expression of major transcriptional regulators confirmed proper cell lineage differentiation in

321 the *Zdbf2*-KO developing pituitary (Figure S6B) (Raetzman *et al*, 2002; Rizzoti, 2015;

322 Kelberman *et al*, 2009). Immunohistochemistry at E18.5 further indicated that *Zdbf2*-KO

323 pituitary cells acquire normal competency for producing hormones (Figure S6D). Similarly,
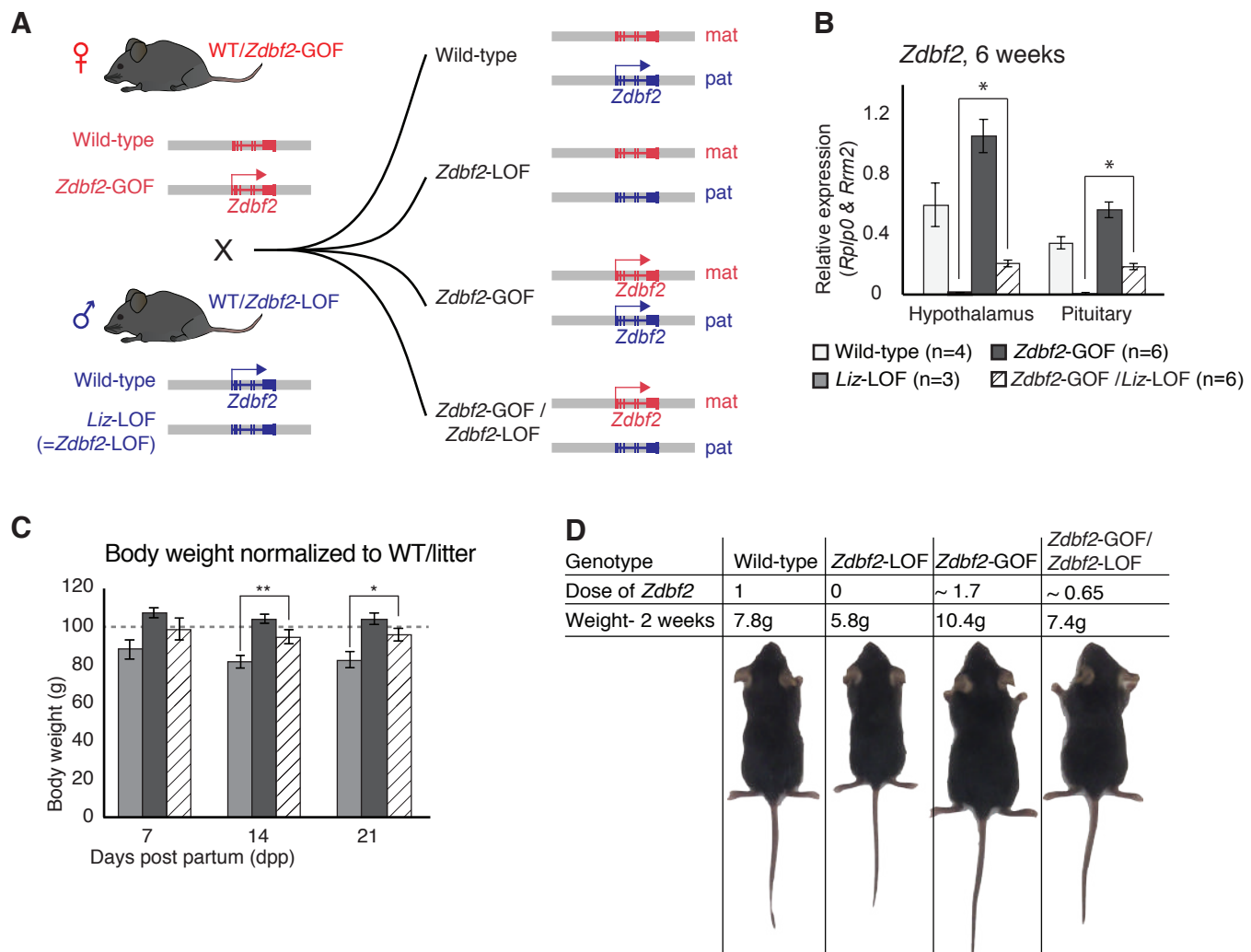
Glaser et al. _Figure 4

Figure 4: *Zdbf2* **influences postnatal growth in a parent-of-origin-independent manner.**
(**A**) Scheme of the cross made to obtain embryos with an inversion of the parental origin of *Zdbf2* expression. *Zdbf2*-GOF heterozygote females were crossed with heterozygote males for the *Liz*-LOF deletion- which we demonstrated as equivalent to a *Zdbf2*-LOF allele- (left) to obtain one quarter of embryos expressing one dose of *Zdbf2* from the maternal allele (right, bottom). (**B**) *Zdbf2* expression in the hypothalamus and the pituitary gland is shown in males for each of the four possible genotypes. The level of *Zdbf2* in *Zdbf2*-GOF /*Zdbf2*-LOF mice almost completely rescues the defect seen in *Zdbf2*-LOF and *Zdbf2*-GOF mutants. Data are shown as means ± s.e.m. from n individuals. Statistical analyses were performed by a two-tailed, unpaired, nonparametric Mann Whitney t test. * $p \leq$ 0.05. (**C**) Normalized body growth of *Zdbf2*-LOF, *Zdbf2*-GOF and *Zdbf2*-GOF /*Zdbf2*-LOF males to their WT littermates (100%) followed at 7, 14 and 21 days after birth. *Zdbf2*-GOF /*Zdbf2*-LOF adult mice exhibit a body weight similar to the WT showing a partial rescue of the growth reduction and overgrowth phenotype due to respectively the lack of *Zdbf2* and the gain of *Zdbf2* expression in the brain. Data are shown as means ± s.e.m. from individuals from n= 17 litters. Statistical analyses were performed by a two-tailed, unpaired, nonparametric Mann Whitney t test. *$p \leq 0.05$; **$p \leq 0.01$. (**D**) Representative photography of four males littermates from a *Zdbf2*-GOF x *Zdbf2*-LOF cross (as shown in A) at 2 weeks of age. For each animal, genotype, dose of *Zdbf2* expression and weight are indicated.

15

325 hypothalamic peptides were expressed in comparable levels in *Zdbf2*-KO and WT embryos,

326 as assessed by *in situ* hybridization analysis (Figure S6E and S6F) (Biran *et al*, 2015). In sum,

327 the embryonic hypothalamo-pituitary axis develops normally in the absence of *Zdbf2*. Our data

328 implies that the postnatal growth phenotype does not result from impaired establishment or

329 programming of this axis during embryogenesis.

330   We then went on to analyze the functionality of the hypothalamo-pituitary axis in

331 producing hormones after birth. Again, GH, ACTH, TSH, LH and PRL all appeared to be

332 normally expressed in the pituitary glands of *Zdbf2*-KO juvenile animals

333 (immunohistochemistry at 15dpp) (Figure 5A). Although we cannot exclude subtle

334 dysfunctionalities, our results suggest that *Zdbf2* deficiency does not compromise pituitary

335 hormone production. Hormone release was also functional, as we measured normal plasmatic

336 GH levels in 5 and 15dpp *Zdbf2*-KO animals (Figure 5B). We therefore excluded an

337 involvement of GH in the *Zdbf2*-KO growth phenotype.

338   However, *Zdbf2*-KO pups showed reduced plasma circulating levels of insulin growth

339 factor 1 (IGF-1) –a main marker of postnatal growth– which reached only 50% and 20% of WT

340 level at 5dpp and 15dpp, respectively (Figure 5C). In adult mice, the liver is the main site of

341 production of IGF-1, following transcriptional activation under the control of circulating GH

342 (Savage, 2013). In contrast, extrahepatic production of IGF-1 during embryonic and early

343 postnatal life is mostly GH-insensitive (Lupu *et al*, 2001; Kaplan & Cohen, 2007). As mentioned

344 above, decreased IGF-1 levels in juvenile *Zdbf2*-KO animals indeed occurs in the context of

345 normal GH input. Moreover, we measured normal *Igf1* mRNA levels by RT-qPCR in the liver

346 of juvenile *Zdbf2*-KO animals, further illustrating that decreased IGF-1 levels are not a result

347 of altered GH pathway (Figure 5D).

348   The association of low levels of circulating IGF-1 with normal GH secretion prompted

349 us to evaluate more thoroughly the *Zdbf2*-KO growth phenotype. Mouse models of GH

350 deficiency show growth retardation only from 10dpp onwards, while deficiency in IGF-1 affects

351 growth earlier during postnatal development (Lupu *et al*, 2001). When we calculated the growth

352 rate from day 1 to 8 weeks of age, we revealed two distinct phases: *(1)* from 1 to 7dpp, the

353 *Zdbf2* mutant growth rate was 22% lower compared to WT littermates and *(2)* from 15 to 35dpp,

354 the mutant exceeded the WT growth rate (Figure 5E) (catch up phase), showing that the

355 growth defect is exquisitely restrained to the first days of life. More specifically, at the day of

356 birth (1dpp), *Zdbf2*-KO pups were smaller than their WT littermates by 9% (WT 1.41 ± 0.015g,

357 *n*=99; *Zdbf2*-KO 1.29 ± 0.013, *n*=95). After 1 week of post-natal life, the mutant growth

358 restriction reached 18% (WT 3.4 ± 0.13g, *n*=37; *Zdbf2*-KO 2.8 ± 0.11, *n*=17), indicating a failure

359 to thrive prior to 10dpp. Then, at 6 weeks of age, *Zdbf2*-KO animals were smaller than WT by
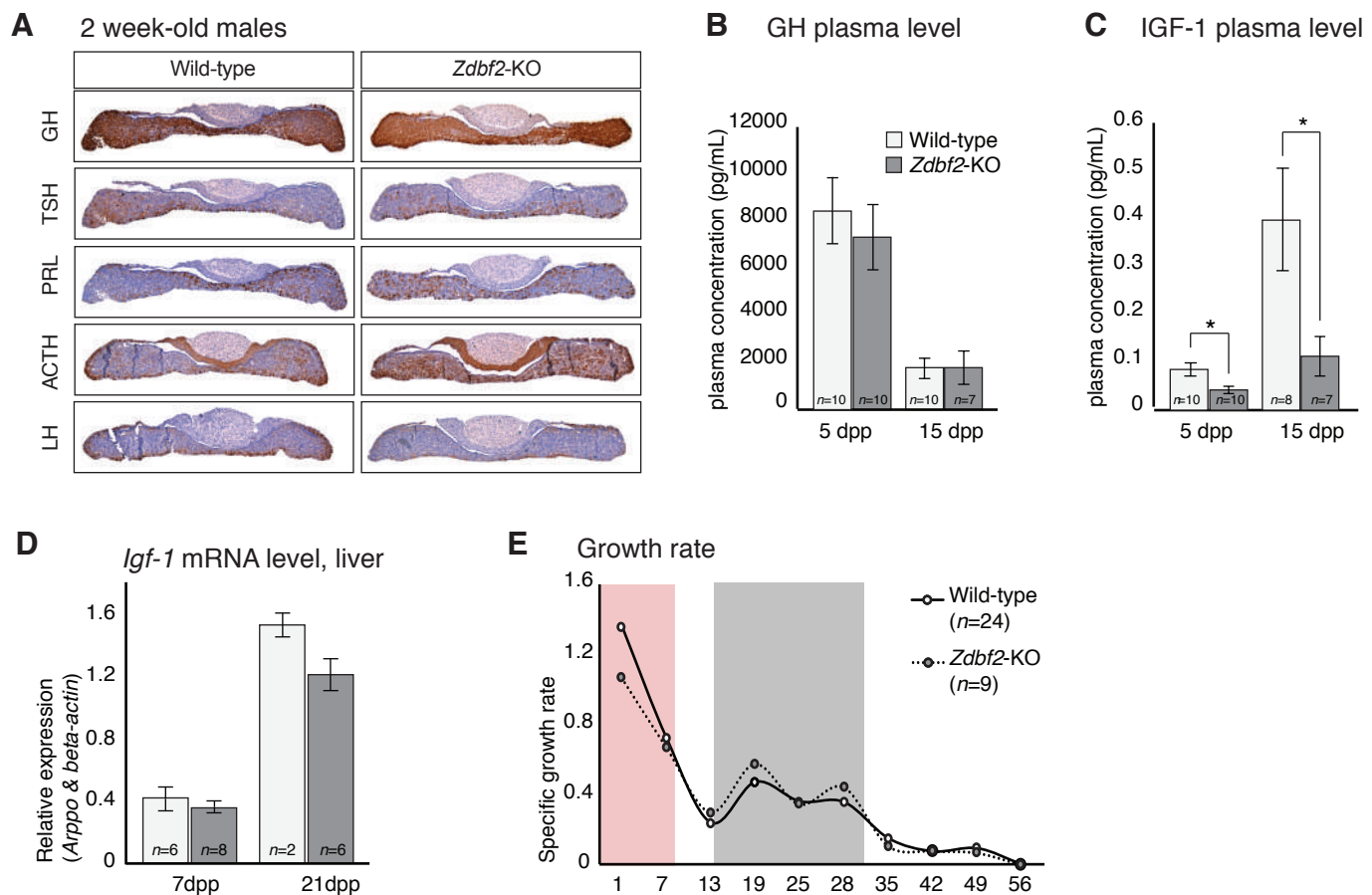
16

Glaser et al._ Figure 5

Figure 5: *Zdbf2*-KO phenotype is linked to defective IGF-1 signaling immediately after birth.
(**A**) Pituitary hormone production is globally normal in *Zdbf2*-KO mice, as assessed by immunohistochemistry on 15dpp pituitary sections. (**B, C**) Circulating levels of GH (**B**) and IGF-1 (**C**) in the plasma of WT and *Zdbf2*-KO mice at 5 and 15dpp. Data are shown as means ± s.e.m. from n replicates. Statistical analyses were performed by a two-tailed, unpaired, nonparametric Mann Whitney t test.*p ≤ 0.05. (**D**) RT-qPCR from post-natal liver measuring the level of *Igf-1* mRNAs between WT and *Zdbf2*-KO mice at 7 and 21dpp. Data are shown as means ±s.e.m from n WT and *Zdbf2*-KO animals. (**E**) Specific growth rates calculated from body weight of WT and *Zdbf2*-KO males from 1 to 56dpp using the following equation: [(weight t2 - weight t1)/ weight t1]. Pink area: reduced growth rate in *Zdbf2*-KO pups compared to WT littermates; Grey area: growth rate of *Zdbf2*-KO mice exceeds the WT growth rate.

361   only 8%, as a result of enhanced post-pubertal growth spurt (WT 21.7 ± 0.04g, *n*=34; *Zdbf2*-

362   KO 20.05 ± 0.3, *n*=15). We therefore concluded that the *Zdbf2*-KO phenotype is similar to

363   defective IGF-1 signaling immediately after birth.

364   Overall, we revealed that the body weight restriction of *Zdbf2*-KO juveniles is

365   associated with a GH-independent decrease of IGF-1 during the first days of postnatal life, in

366   the context of an overall normal development and functionality of the hypothalamo-pituitary

367   axis.

368

369   ***Zdbf2*-KO neonates are undernourished and do not properly activate hypothalamic**

370   **feeding circuits.**

371   Having determined that *Zdbf2*-KO animals exhibit an *Igf-1*-like phenotype, we attempted to

372   define the origin of the GH-independent reduction of IGF-1 levels. Undernutrition is a well-

373   known cause of IGF-1 level reduction, and also of postnatal lethality (Thissen *et al*, 1994),

374   which we observed in *Zdbf2*-KO pups. To investigate the nutritional status of *Zdbf2*-KO

375   neonates, we weighed stomachs at 3dpp, as a measure of milk intake. *Zdbf2*-KO pups

376   exhibited a significant reduction in stomach weight relative to body mass as compared to their

377   WT littermates (Figures 6A and S7A), suggesting that these pups suffer milk deprivation.

378   Comparatively, other organs showed normal relative weight at this age, at the exception of the

379   interscapular brown adipose tissue (BAT), which was also reduced in *Zdbf2*-KO neonates

380   (Figures 6B and S7A). BAT-mediated thermogenesis regulates body heat during the first days

381   after birth (Cannon & Nedergaard, 2004) and improper BAT function can lead to early postnatal

382   death (Charalambous *et al*, 2012). However, despite being smaller, the BAT of *Zdbf2*-KO

383   neonates appeared otherwise functional, showing normal lipid droplet enrichment on

384   histological sections (data not shown) and proper expression of major markers of BAT

385   thermogenic ability (Figure S7B). The BAT size reduction may therefore not reflect altered BAT

386   ontogeny *per se,* but rather the nutritional deprivation of *Zdbf2*-KO neonates.

387   Because the mothers of *Zdbf2*-KO pups are of WT background, the undernutrition

388   phenotype is unlikely due to defective maternal milk supply. Restoration of viability when

389   placed in presence of KO-only littermates (Figure 2K) further indicated that *Zdbf2*-KO pups are

390   competent for suckling. Defective nutrition may therefore rather result from altered feeding

391   motivation of the *Zdbf2*-KO neonates, specifically during the early nursing period. To test this

392   hypothesis, we performed RNA-seq analysis of dissected hypothalami at 3dpp, when the

393   growth phenotype is the most acute (Figure 6C). Only 11 genes were significantly

394   misexpressed in the *Zdbf2*-KO pups relative to their WT littermates (FDR 10%), with a majority

395   being downregulated genes, including *Npy*, which encodes the Neuropeptide Y. In line with

396   our hypothesis, NPY is secreted from neurons of the hypothalamic arcuate nucleus, where

397   *Zdbf2* is expressed and stimulates food intake and promotes gain weight (Mercer *et al*, 2011).

398   Little is known about the determinants of food intake in neonates (Muscatelli & Bouret, 2018),

399   nonetheless, this prompted us to examine the expression levels of other hypothalamic

400   modulators known to influence feeding behavior in adults. Interestingly, *Zdbf2*-KO pups

401   showed a trend towards downregulation of the Agouti-related peptide (*Agrp*)-encoding gene

402   (Figure 6D), which is co-expressed with *Npy* in a sub-population of hypothalamic neurons and

403   convergently stimulate appetite and food seeking (Gropp *et al*, 2005). It is noteworthy that

404   none of the misregulated genes –including positive regulators of feeding– that we observed at

405   3dpp were continuously misregulated in the hypothalamus at 10dpp, when *Zdbf2*-KO pups

406   enter the catch-up phase (Figure S7C and S7D).

407   Together, these results provide key insights into the origin of the *Zdbf2* mutant

408   phenotype: in absence of *Zdbf2,* the hypothalamic circuit of genes that stimulates food intake

409   may not be properly activated at birth. This is associated with reduced milk intake, reduced

410   body weight gain and suboptimal viability of *Zdbf2*-KO neonates when placed in presence of
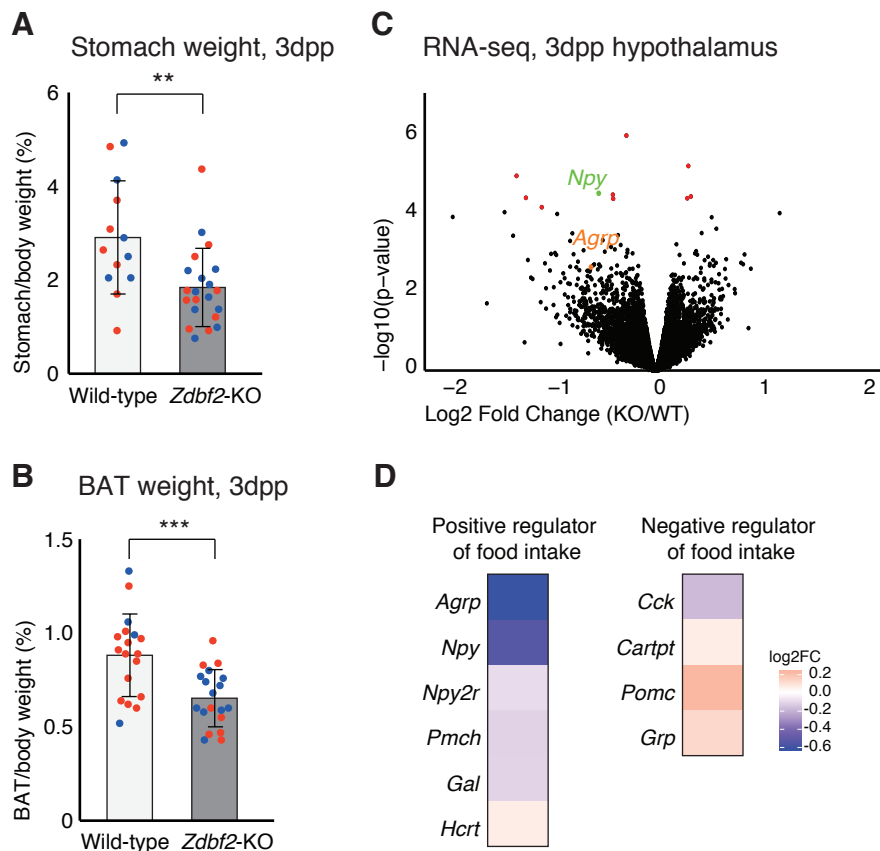
411   healthier littermates.

Glaser et al._ Figure 6

A

Stomach weight, 3dpp

B

BAT weight, 3dpp

C

RNA-seq, 3dpp hypothalamus

D

Figure 6: *Zdbf2*-KO neonates display a feeding defect.

(**A, B**) Stomach (**A**) and brown adipocyte tissue (BAT) (**B**) weight normalized to the body weight for WT and *Zdbf2*-KO at 3dpp. Red dots: females; blue dots: males. Data are shown as means ± s.e.m. from n replicates. Statistical analyses were performed by a two-tailed, unpaired, nonparametric Mann Whitney t test.** p≤ 0.01, ***p ≤ 0.005. (**C**) Volcano plot representation of RNA-seq of 3dpp hypothalamus of *Zdbf2*-KO versus WT littermates. Red dots: differentially expressed genes with a threshold of FDR<10%. Npy (FDR 6%) is highlighted in green and Agrp in orange. (**D**) Heatmap showing the log2 fold change of genes encoding hypothalamic regulators of food intake (RNA-seq data from C).

20

DISCUSSION

The hypothalamus is increasingly regarded as a major site for the action of imprinted genes on postnatal growth, feeding behavior and metabolism (Ivanova & Kelsey, 2011). Here, we found evidence that the imprinted *Zdbf2* gene stimulates hypothalamic feeding circuits, right after birth. In its absence, neonates do not suckle enough milk, and suffer from undernutrition. This leads to decreased IGF-1 signaling within the first week of life, reduced body weight gain and more dramatically, lethality of half of the *Zdbf2*-KO pups when they are in presence of healthier WT littermates. Our work therefore highlights that *Zdbf2* is necessary to thrive and survive after birth, by allowing newborns to adapt to postnatal feeding.

By relying on a unique collection of mouse models of total loss of function (*Zdbf2*-KO and *Liz-LOF*), partial loss of function (*Zdbf2*-lacZ), normal function (*Zdbf2*-WT) and gain of function (*Zdbf2*-GOF), we observed that postnatal body growth is exquisitely sensitive to the quantity of *Zdbf2* produced in the hypothalamo-pituitary axis. Incidentally, *Zdbf2* meets the criteria of a *bona fide* growth-promoting gene: growth is reduced upon decreased dosage and oppositely enhanced upon increased dosage of *Zdbf2* (Efstratiadis, 1998). Consistent with previous results for the imprinted *Cdkn1c* gene (Andrews *et al*, 2007), growth reduction was more pronounced than overgrowth upon changes in *Zdbf2* expression (18% decrease and 10% increase at 10dpp) and specific to males. This reflects that, with standard diet, overgrowth is a much less frequent response than growth reduction and affects animals with favorable physiology only, potentially explaining male specificity.

With a few exceptions, most studies have only addressed the phenotypic effects of reducing the dose of an imprinted gene, but not what results from overexpressing this same gene (Tucci *et al*, 2019). Knocking out an imprinted gene provides valuable insights about its physiological function, however, it does not address the evolutionary significance of imprinting of that gene, *i.e.* reduction to mono-allelic expression. With the *Zdbf2*-GOF model, we were able to evaluate the consequences of a loss of *Zdbf2* imprinting: bi-allelic and increased *Zdbf2* expression exacerbates postnatal body weight gain. However, despite being slightly bigger, viability, fertility or longevity appeared overall normal in *Zdbf2*-GOF animals. The evolutionary importance of *Zdbf2* imprinting is therefore not immediately obvious, at least under unchallenged conditions. Finally, even fewer studies have addressed the importance of parent-of-origin expression for imprinted gene functions (Drake *et al*, 2009; Leighton *et al*, 1995). By intercrossing models of *Zdbf2* loss and gain of function, we could enforce *Zdbf2* expression from the maternal allele while inactivating the normally expressed paternal allele. Restoration of body weight demonstrated the functionality of maternal *Zdbf2* expression, validating that *Zdbf2* functions on postnatal body homeostasis in a dose-dependent but parent-of-origin-

21

448 independent manner. Although not necessarily surprising, this demonstration is conceptually

449 important for understanding the evolution and *raison d'être* of genomic imprinting. The

450 divergent DNA methylation patterns that are established in the oocyte and the spermatozoa

451 provide opportunities to evolve mono-allelic regulation of expression, but the parental

452 information is not essential *per se*.

453   Although *Zdbf2* is expressed across the hypothalamo-pituitary axis, we could not find

454 evidence of abnormal development or function of the pituitary gland that could explain the

455 *Zdbf2*-KO growth phenotype. Notably, GH production and release was normal. Additionally,

456 the *Zdbf2* growth reduction diverges from GH-related dwarfism: *Gh*-deficient mice grow

457 normally until 10dpp, after which only they exhibit general growth impairment with reduced

458 levels of circulating IGF-1 (Voss & Rosenfeld, 1992; Lupu *et al*, 2001). In *Zdbf2*-KO mutants,

459 the growth defect is apparent as soon as 1dpp and we measured decreased IGF-1 at 5 dpp.

460 In *Igf-1* null mice, birthweight is approximately 60% of normal weight and some mutants die

461 within the first hours after birth (Liu *et al*, 1993; Efstratiadis, 1998). The *Zdbf2*-KO phenotype

462 thus resembles an attenuated *Igf-1* deficiency, in agreement with half reduction but not total

463 lack of circulating IGF-1. Interestingly, similar IGF-1-related growth defects have been reported

464 upon alteration of other imprinted loci: the *Dlk1-Dio3* cluster and the *Cdkn1c* gene (Andrews

465 *et al*, 2007; Charalambous *et al*, 2014). Finally, decreased *ZDBF2* levels have recently been

466 associated with intra-uterine growth restriction (IUGR) in humans (Monteagudo-Sánchez *et al*,

467 2019). Whether this is linked to impaired fetal IGF-1 production would be interesting to assess.

468   IGF-1 secretion has been shown to drop in response to starvation, leading to disturbed

469 growth physiology (Savage, 2013). Our findings support that limited food intake is probably the

470 primary defect in *Zdbf2* deficiency, leading to IGF-I insufficiency in the critical period of

471 postnatal development and consequently, growth restriction. First, we showed that *Zdbf2* is

472 expressed in hypothalamic regions that contain neurons with functions in appetite and food

473 intake regulation, such as the arcuate and paraventricular nucleus. Second, *Zdbf2-KO*

474 neonates show hypothalamic downregulation of the *Npy* and *Agrp* genes that encode for

475 orexigenic neuropeptides (Stanley & Leibowitz, 1984; Ollmann *et al*, 1997). These are likely

476 direct effects, as the rest of the hypothalamic transcriptome is scarcely modified in *Zdbf2*-KO

477 pups. Quantified changes in RNA-seq were not of large magnitude (although significant for

478 *Npy*), but AgRP/NPY neurons represent a very small population of cells, present in the arcuate

479 nucleus of the hypothalamus only (Andermann & Lowell, 2017). We are likely at the limit of

480 detection when analyzing these genes in the whole hypothalamus transcriptome. Finally, *Npy*

481 and *Agrp* downregulation was observed as early as 3 days after birth, along with a phenotype

482 of reduced milk consumption, as measured by stomach weighing. Given our observations, we

483 propose that ZDBF2 activates specialized hypothalamic neurons that motivate neonates to
484 actively demand food (milk) from the mother right at birth, promoting the transition to oral
485 feeding after a period of passive food supply *in utero*. This function agrees with the co-
486 adaptation theory according to which genomic imprinting evolved to coordinate interactions
487 between the offspring and the mother (Wolf & Hager, 2006). Despite considerable effort, we
488 were unable to specifically detect the ZDBF2 protein with antibodies or using epitope-tagging
489 approaches of the endogenous gene; future studies hopefully will bring clarity to which
490 molecular function ZDBF2 carries in the hypothalamus.

491 In conclusion, we reveal here that decreasing *Zdbf2* compromises resource acquisition
492 and body weight gain right after birth. Restricted postnatal growth can have a strong causal
493 effect on metabolic phenotypes, increasing the risk of developing obesity in later life. This is
494 observed in mouse KO models of the imprinted *Magel2* gene that maps to the Prader Willi
495 syndrome region, and in PWS children themselves, who after a failure to thrive as young
496 infants exhibit a catch-up phase leading to overweight and hyperphagia (Bischof *et al*, 2007).
497 *Zdbf2*-KO mice do present a post-puberal spurt of growth, which attenuates their smaller body
498 phenotype, but we never observed excessive weight gain, even after 18 months. It would be
499 interesting to test whether the restricted postnatal growth of *Zdbf2*-KO mice may nonetheless
500 increase the likelihood of metabolic complications when challenged with high-fat or high sugar
501 diet.

MATERIALS AND METHODS

Mice

Mice were hosted on a 12 h/12 h light/dark cycle with free access to food and water in the pathogen-free Animal Care Facility of the Institut Curie (agreement number: C 75-05-18). All experimentation was approved by the Institut Curie Animal Care and Use Committee and adhered to European and National Regulation for the Protection of Vertebrate Animals used for Experimental and other Scientific Purposes (Directive 86/609 and 2010/63). For tissue and embryo collection, euthanasia was performed by cervical dislocation. The *Zdbf2*-KO and *Zdbf2*-GOF mutant mice lines were derived by CRISPR/Cas9 engineering in one-cell stage embryos as previously described (Greenberg *et al*, 2017), using two deletion-promoting sgRNAs. Zygote injection of the CRISPR/Cas9 system was performed by the Transgenesis Platform of the Institut Curie. Eight week-old superovulated C57BL/6J females were mated to stud males of the same background. Cytoplasmic injection of Cas9 mRNA and sgRNAs (100 and 50 ng/ul, respectively) was performed in zygotes collected in M2 medium (Sigma) at E0.5, with well-recognized pronuclei. Injected embryos were cultured in M16 medium (Sigma) at 37°C under 5% CO_2, until transfer at the 1-cell stage the same day or at the 2-cell stage the following day in the infudibulum of the oviduct of pseudogestant CD1 females at E0.5. The founder mice were then genotyped and two independent founders with the expected deletion were backcrossed to segregate out undesired genetic events, with a systematic breeding scheme of *Zdbf2*-KO heterozygous females x WT C57Bl6/J males and *Zdbf2*-GOF heterozygous males x WT C57Bl6/J females to promote silent passing of the deletion. Cohorts of female and male N3 animals were then mated with WT C57Bl6/J to study the maternal and paternal transmission of the mutation.

The LacZ-*Zdbf2* reporter mouse line was derived from mouse embryonic stem (ES) cells from the European Conditional Mouse Mutagenesis Program (EUCOMM Project Number: *Zdbf2*_82543). Proper insertion of the LacZ construct was confirmed by long range PCR. However, upon Sanger sequencing, we found that the loxP site in the middle position was mutated (A to G transition at position 16 of the loxP site) in the original ES cells (Figure S4A). Chimeric mice were generated through blastocyst injection by the Institut Curie Transgenesis platform. We studied animals with an intact LacZ-KI allele, without FRT- or CRE-induced deletions.

DNA methylation analyses

24

535 Genomic DNA from adult tissues was obtained following overnight lysis at 50°C (100mM Tris
536 pH 8, 5mM EDTA, 200mM NaCl, 0.2% SDS and Proteinase K). DNA was recovered by a
537 standard phenol/choloroform/isoamyl alcohol extraction and resuspended in water. Bisulfite
538 conversion was performed on 0.5-1ug of DNA using the EpiTect Bisulfite Kit (Qiagen). Bisulfite-
539 treated DNA was PCR amplified and either cloned and sequenced, or analyzed by
540 pyrosequencing. For the former, 20-30 clones were Sanger sequenced and analyzed with BiQ
541 Analyzer software (Bock *et al*, 2005). Pyrosequencing was performed on the PyroMark Q24
542 (Qiagen) according to the manufacturer's instructions, and results were analyzed with the
543 associated software.

544

545 **RNA expression analyses**

546 Total RNA was extracted using Trizol (Life Technologies). To generate cDNA, 1ug of Trizol-
547 extracted total RNA was DNase-treated (Ambion), then reverse transcribed with SuperscriptIII
548 (Life Technologies) primed with random hexamers. RT-qPCR was performed using the SYBR
549 Green Master Mix on the ViiA7 Real-Time PCR System (Thermo Fisher Scientific). Relative
550 expression levels were normalized to the geometric mean of the Ct for housekeeping genes
551 *Rrm2*, *B-actin* and/or *Rplp0*, with the ΔΔCt method. Primers used are listed in Supplemental
552 Table 2.

553 For RNA-sequencing, hypothalamus of three animals at 3dpp and two animals at 10dpp were
554 collected for each genotype and RNA was extracted. Trizol-extracted total RNA was DNase-
555 treated with the Qiagen RNase-Free DNase set, quantified using Qubit Fluorometric
556 Quantitation (Thermo Fisher Scientific) and checked for integrity using Tapstation. RNA-seq
557 libraries were cloned using TruSeq Stranded mRNA LT Sample Kit on total RNA (Illumina) and
558 sequencing was performed in 100bp paired-end reads run on a NovaSeq (Illumina) at the
559 NGS platform of the Institut Curie.

560

561 **LacZ staining**

562 Whole brains and pituitary glands were fixed in 4% paraformaldehyde (PFA) in PBS (pH 7.2)
563 overnight and washed in PBS. For sections, tissues were then incubated in sucrose gradients
564 and embedded in OCT for conservation at -80°C before cryosectioning. Sections were first
565 fixed 10 minutes in solution of Glutaraldehyde (0.02% Glutaraldehyde, 2mM MgCl2 in PBS).
566 Tissues and sections were washed in washing solution (2mM MgCl2, 0.02% NP40, 0.01%
567 $C_{24}H_{39}NaO_4$ in PBS) and finally incubated at room temperature overnight in X- gal solution
568 (5mM $K_4Fe(CN)_63H_2O$, 5mM $K_3Fe(CN)_6$, 25mg/mL X-gal in wash solution). After several PBS

25

569   washes, sections were mounted with an aqueous media and conserved at room temperature

570   before imaging.

571

Histological analysis and RNA *in situ* hybridization

573   Embryos at E13.5 and E15.5 were embedded in paraffin and sectioned at a thickness of 5 μm.

574   For histological analysis, paraffin sections were stained with Haematoxylin and Eosin. RNA *in*

575   *situ* hybridization analysis on paraffin sections was performed following a standard procedure

576   with digoxigenin-labeled antisense riboprobes as previously described (Gaston-Massuet *et al*,

577   2008).The antisense riboprobes used in this study [α-Gsu, *Pomc1*, *Lhx3*, *Pitx1, Avp, oxytocin*

578   *and Ghrh*] have been previously described (Gaston-Massuet *et al*, 2008, 2016).

579

Immunohistochemistry on histological sections

581   Embryos were fixed in 4% PFA and processed for immuno- detection as previously described

582   (Andoniadou *et al*, 2013). Detection of hormones was carried out using antibodies for α-GH

583   (rabbit polyclonal, NHPP AFP-5641801, 1:1000), α-TSH (rabbit polyclonal, NHPP AFP-

584   1274789, 1:1000), α-PRL (rabbit polyclonal, NHPP AFP-425-10-91, 1:1000), α-ACTH (mouse

585   monoclonal, 10C-CR1096M1, 1:1000) and α-LH (rabbit polyclonal, NHPP AFP-C697071P,

586   1:500).

587

LUMINEX ELISA assay

589   Plasma from blood was collected in the morning at fixed time on EDTA from 5 and 15 day-

590   old mice after euthanasia and stored at -20C until use. Samples were run in duplicates using

591   the Mouse Magnetic Luminex Assay for IGF-1 (R&D System) and Milliplex Mouse Pituitary

592   Magnetic Assay for GH (Merck) according to manufacturers' instructions. Values were read

593   on Bio-Plex® 200 (Bio-Rad) and analyzed with the Bio-Plex Manager Software.

594

Phenotypic analyses of weight

596   Postnatal weight measurements were performed every two days from 1dpp to weaning age

597   (21 days). Then, mice were separated according to their genotype, hosted in equal number

598   per cage (*n*=5 to 6) and weighted once per week. As body weight is a continuous variable, we

599   used a formula derived from the formula for the *t*-test to compute the minimum sample size

600   per genotype: $n=1+C(s/d)^2$, where *C* is dependent on values chosen for significance level (α)

601 and power (1-β), *s* is the standard deviation and *d* the expected difference in means. Using α

602 =5%, β=90% and an expected difference in means of 1g at 2 weeks and 2g later on, we

603 predicted a minimum *n* of between 10 and 20 and thus decided to increase this number using

604 *n* size between 20 and 30 per genotype, depending of the age and the sex of the mice. No

605 animals were excluded from the analysis. Animals were blindly weighed until genotyping at

606 weaning age. E18.5 embryos and post-natal organs were collected and individually, rinsed in

607 PBS and weighted on a 0.001g scale. All data were generated using three independent mating

608 pairs.

609

610 **Phenotypic analyses of post-natal lethality**

611 Material for genotyping was taken the first day of birth and then number of pups for a given

612 litter was assessed every day. To avoid bias, we excluded from the analysis the litters where

613 all the pups died due to neglecting mothers, not taking care of their pups.

614

615 **DEXA scan analyses**

616 The DEXA analysis allows the assessment of fat and lean mass, bone area, bone mineral

617 content and bone mineral density. Practically, mutant and WT littermate males at 2 weeks

618 were sent from the Animal Facility of Institut Curie to the Mouse Clinics along with their mother

619 (Ilkirch, France). The phenotypic DEXA analysis was performed at 7 weeks of age using an

620 *Ultrafocus DXA* digital radiography system, after the mandatory 5 week-quarantine period in

621 the new animal facility. Mice were anesthetized prior analysis and scarified directly after

622 measurements, without a waking up phase.

623

624 **RNA- seq data analysis**

625 Adapters sequences were trimmed using TrimGalore v0.6.2

626 (https://github.com/FelixKrueger/TrimGalore). Paired-end reads were mapped using

627 STAR_2.6.1a (Dobin *et al*, 2012) allowing 4% of mismatches. Gencode vM13 annotation was

628 used to quantify gene expression using quantification mode from STAR. Normalization and

629 differential gene expression were performed using EdgeR R package (v3.22.3)(Robinson *et*

630 *al*, 2009). Genes were called as differentially expression if the fold discovery rate (FDR) is

631 lower than 10%.

632

633 **Statistical Analyses**

27

634   Significance of obtained data was determined by performing two-tailed unpaired,

635   nonparametric Mann Whitney t- tests using GraphPad Prism6 software. p values were

636   considered as significant when $p \leq 0.05$. Data points are denoted by stars based on their

637   significance: **** : $p \leq 0.0001$; *** : $p \leq 0.001$; ** : $p \leq 0.01$; * : $p \leq 0.05$.

638

639   **Data availability**

640   The datasets produced in this study are available in the following databases:

641   RNA-Seq data: Gene Expression Omnibus GSE153265

642   (https://www.ncbi.nlm.nih.gov/geo/query/acc.cgi?acc=GSE153265).

ACKNOWLEDGEMENTS

AUTHOR CONTRIBUTION

Conceptualization: D.B. and J.G; Methodology: D.B., J.G. and C.G.M. Formal analysis: J.G. and A.T.; Investigations: J.G., J.I., M.B., M.M., C.J., A.G.; Writing: J.G. and D.B.; Supervision: D.B.; Funding acquisition: D.B. and C.G.M.

COMPETING INTERESTS

The authors declare that they have no competing interests.

REFERENCES

Andermann ML & Lowell BB (2017) Toward a Wiring Diagram Understanding of Appetite Control. *Neuron* **95:** 757–778

Andoniadou CL, Matsushima D, Mousavy Gharavy SN, Signore M, Mackintosh AI, Schaeffer M, Gaston-Massuet C, Mollard P, Jacques TS, Le Tissier P, Dattani MT, Pevny LH & Martinez-Barbera JP (2013) Sox2+ Stem/Progenitor Cells in the Adult Mouse Pituitary Support Organ Homeostasis and Have Tumor-Inducing Potential. *Cell Stem Cell* **13:** 433–445 Available at: https://doi.org/10.1016/j.stem.2013.07.004

Andrews SC, Wood MD, Tunster SJ, Barton SC, Surani MA & John RM (2007) Cdkn1c (p57Kip2) is the major regulator of embryonic growth within its imprinted domain on mouse distal chromosome 7. *BMC Dev. Biol.* **7:** 53 Available at: https://pubmed.ncbi.nlm.nih.gov/17517131

Biran J, Tahor M, Wircer E & Levkowitz G (2015) Role of developmental factors in hypothalamic function. *Front. Neuroanat.* **9:** 1–11

Bischof JM, Stewart CL & Wevrick R (2007) Inactivation of the mouse Magel2 gene results in growth abnormalities similar to Prader-Willi syndrome. *Hum. Mol. Genet.* **16:** 2713–2719

Bock C, Reither S, Mikeska T, Paulsen M, Walter J & Lengauer T (2005) BiQ Analyzer: Visualization and quality control for DNA methylation data from bisulfite sequencing. *Bioinformatics* **21:** 4067–4068

Bogutz AB, Brind'Amour J, Kobayashi H, Jensen KN, Nakabayashi K, Imai H, Lorincz MC & Lefebvre L (2019) Evolution of imprinting via lineage-specific insertion of retroviral promoters. *Nat. Commun.* **10:** 5674 Available at: https://doi.org/10.1038/s41467-019-13662-9

Buiting K (2010) Prader-Willi syndrome and Angelman syndrome. *Am. J. Med. Genet. C. Semin. Med. Genet.* **154C:** 365–376

Cannon B & Nedergaard J (2004) Brown Adipose Tissue: Function and Physiological Significance. *Physiol. Rev.* **84:** 277–359 Available at: https://doi.org/10.1152/physrev.00015.2003

Cassidy SB & Driscoll DJ (2009) Prader–Willi syndrome. *Eur. J. Hum. Genet.* **17:** 3–13 Available at: https://doi.org/10.1038/ejhg.2008.165

Charalambous M, Ferron SR, Da Rocha ST, Murray AJ, Rowland T, Ito M, Schuster-Gossler K, Hernandez A & Ferguson-Smith AC (2012) Imprinted gene dosage is critical for the transition to independent life. *Cell Metab.* **15:** 209–221

Charalambous M, Rocha ST, Hernandez A & Ferguson-smith AC (2014) Perturbations to the IGF1 growth pathway and adult energy homeostasis following disruption of mouse chromosome 12 imprinting. *Acta Physiol* **210:** 174–187

Chen R, Wu X, Jiang L & Zhang Y (2017) Single-Cell RNA-Seq Reveals Hypothalamic Cell Diversity. *Cell Rep.* **18:** 3227–3241

Chen W, Wilson JL, Khaksari M, Cowley MA & Enriori PJ (2012) Abdominal fat analyzed by DEXA scan reflects visceral body fat and improves the phenotype description and the assessment of metabolic risk in mice. *AJP Endocrinol. Metab.* **303:** E635–E643

Cheung LYM, George AS, McGee SR, Daly AZ, Brinkmeier ML, Ellsworth BS & Camper SA (2018) Single-Cell RNA Sequencing Reveals Novel Markers of Male Pituitary Stem Cells and Hormone-Producing Cell Types. *Endocrinology* **159:** 3910–3924

Dobin A, Davis CA, Schlesinger F, Drenkow J, Zaleski C, Jha S, Batut P, Chaisson M & Gingeras TR (2012) STAR: ultrafast universal RNA-seq aligner. *Bioinformatics* **29:** 15–21 Available at: https://doi.org/10.1093/bioinformatics/bts635

Drake NM, Park JY, Shirali AS, Cleland TA & Soloway PD (2009) Imprint switch mutations at Rasgrf1 support conflict hypothesis of imprinting and define a growth control mechanism upstream of IGF1. *Mamm. Genome* **20:** 654–663

Duffié R, Ajjan S, Greenberg M V., Zamudio N, del Arenal Escamilla M, Iranzo J, Okamoto I, Barbaux S, Fauque P & Bourc'his D (2014) The Gpr1/Zdbf2 locus provides new paradigms for transient and dynamic genomic imprinting in mammals. *Genes Dev.* **28:**

463–478

Efstratiadis A (1998) Genetics of mouse growth. *Int. J. Dev. Biol.* **42:** 955–976

Ferrón SR, Charalambous M, Radford E, McEwen K, Wildner H, Hind E, Morante-Redolat JM, Laborda J, Guillemot F, Bauer SR, Fariñas I & Ferguson-Smith AC (2011) Postnatal loss of Dlk1 imprinting in stem cells and niche astrocytes regulates neurogenesis. *Nature* **475:** 381–387

Gaston-Massuet C, Andoniadou CL, Signore M, Sajedi E, Bird S, Turner JMA & Martinez-Barbera JP (2008) Genetic interaction between the homeobox transcription factors HESX1 and SIX3 is required for normal pituitary development. *Dev. Biol.* **324:** 322–333 Available at: http://www.sciencedirect.com/science/article/pii/S0012160608011196

Gaston-Massuet C, McCabe MJ, Scagliotti V, Young RM, Carreno G, Gregory LC, Jayakody SA, Pozzi S, Gualtieri A, Basu B, Koniordou M, Wu C-I, Bancalari RE, Rahikkala E, Veijola R, Lopponen T, Graziola F, Turton J, Signore M, Mousavy Gharavy SN, et al (2016) Transcription factor 7-like 1 is involved in hypothalamo-pituitary axis development in mice and humans. *Proc. Natl. Acad. Sci. U. S. A.* **113:** E548-57

Greenberg M, Teissandier A, Walter M, Noordermeer D & Bourc'his D (2019) Dynamic enhancer partitioning instructs activation of a growth-related gene during exit from naïve pluripotency. *Elife* **8:** e44057 Available at: https://doi.org/10.7554/eLife.44057

Greenberg MVC, Glaser J, Borsos M, Marjou F El, Walter M, Teissandier A & Bourc'his D (2017) Transient transcription in the early embryo sets an epigenetic state that programs postnatal growth. *Nat. Genet.* **49:** 110–118

Gregg C, Zhang J, Weissbourd B, Luo S, Schroth GP, Haig D & Dulac C (2010) High-resolution analysis of parent-of-origin allelic expression in the mouse brain. *Science* **329:** 643–648

Gropp E, Shanabrough M, Borok E, Xu AW, Janoschek R, Buch T, Plum L, Balthasar N, Hampel B, Waisman A, Barsh GS, Horvath TL & Brüning JC (2005) Agouti-related peptide–expressing neurons are mandatory for feeding. *Nat. Neurosci.* **8:** 1289–1291 Available at: https://doi.org/10.1038/nn1548

Haig D (2000) The Kinship Theory of Genomic Imprinting. *Annu. Rev. Ecol. Syst.* **31:** 9–32 Available at: https://doi.org/10.1146/annurev.ecolsys.31.1.9

Ivanova E & Kelsey G (2011) Imprinted genes and hypothalamic function. *J. Mol. Endocrinol.* **47:**

Kaplan SA & Cohen P (2007) REVIEW: The Somatomedin Hypothesis 2007: 50 Years Later. *J. Clin. Endocrinol. Metab.* **92:** 4529–4535 Available at: https://doi.org/10.1210/jc.2007-0526

Kelberman D, Rizzoti K, Lovell-Badge R, Robinson ICAF & Dattani MT (2009) Genetic regulation of pituitary gland development in human and mouse. *Endocr. Rev.* **30:** 790–829

Kobayashi H, Yamada K, Morita S, Hiura H, Fukuda A, Kagami M, Ogata T, Hata K, Sotomaru Y & Kono T (2009) Identification of the mouse paternally expressed imprinted gene Zdbf2 on chromosome 1 and its imprinted human homolog ZDBF2 on chromosome 2. *Genomics* **93:** 461–472

Kozlov S V, Bogenpohl JW, Howell MP, Wevrick R, Panda S, Hogenesch JB, Muglia LJ, Van Gelder RN, Herzog ED & Stewart CL (2007) The imprinted gene Magel2 regulates normal circadian output. *Nat. Genet.* **39:** 1266–1272

Leighton PA, Ingram RS, Eggenschwiler J, Efstratiadis A & Tilghman SM (1995) Deletion of the H19 gene region in mice disrupts the imprinting of its neighbouring genes. *Nature* **375:** 34–39

Li L-L, Keverne EB, Aparicio SA, Ishino F, Barton SC & Surani MA (1999) Regulation of Maternal Behavior and Offspring Growth by Paternally Expressed Peg3. *Science* **284:** 330–334

Li X, Ito M, Zhou F, Youngson N, Zuo X, Leder P & Ferguson-Smith AC (2008) A Maternal-Zygotic Effect Gene, Zfp57, Maintains Both Maternal and Paternal Imprints. *Dev. Cell* **15:** 547–557

771 Liu J-P, Baker J, Perkins AS, Roberteon EJ & Efetratiadis A (1993) Mice carrying null
772   mutations of the genes encoding insulinlike growth factor I (lgt-1) and type 1 IGF
773   receptor (lgf1r). *Cell* **75:** 59–72

774 Lupu F, Terwilliger J & Lee K (2001) Roles of growth hormone and insulin-like growth factor
775   1 in mouse postnatal growth. *Dev. Biol.* **229:** 141–162

776 Mercer RE, Chee MJS & Colmers WF (2011) The role of NPY in hypothalamic mediated food
777   intake. *Front. Neuroendocrinol.* **32:** 398–415 Available at:
778   http://www.sciencedirect.com/science/article/pii/S0091302211000537

779 Mollard P, Hodson DJ, Lafont C, Rizzoti K & Drouin J (2012) A tridimensional view of
780   pituitary development and function. *Trends Endocrinol. Metab.* **23:** 261–269

781 Monteagudo-Sánchez A, Sánchez-Delgado M, Mora JRH, Santamaría NT, Gratacós E,
782   Esteller M, de Heredia ML, Nunes V, Choux C, Fauque P, de Nanclares GP, Anton L,
783   Elovitz MA, Iglesias-Platas I & Monk D (2019) Differences in expression rather than
784   methylation at placenta-specific imprinted loci is associated with intrauterine growth
785   restriction. *Clin. Epigenetics* **11:** 35 Available at: https://doi.org/10.1186/s13148-019-
786   0630-4

787 Muscatelli F & Bouret SGC (2018) Wired for eating: how is an active feeding circuitry
788   established in the postnatal brain? *Curr. Opin. Neurobiol.* **52:** 165–171 Available at:
789   http://www.sciencedirect.com/science/article/pii/S0959438818300862

790 Nagy TR & Clair AL (2000) Precision and accuracy of dual-energy X-ray absorptiometry for
791   determining in vivo body composition of mice. *Obes. Res.* **8:** 392–398

792 Nicholls RD, Knoll JHM, Butler MG, Karam S & Lalande M (1989) Genetic imprinting
793   suggested by maternal heterodisomy in non-deletion Prader-Willi syndrome. *Nature*
794   **342:** 281–285 Available at: https://doi.org/10.1038/342281a0

795 Ollmann MM, Wilson BD, Yang Y-K, Kerns JA, Chen Y, Gantz I & Barsh GS (1997)
796   Antagonism of Central Melanocortin Receptors in Vitro and in Vivo by Agouti-Related
797   Protein. *Science* **278:** 135 LP – 138 Available at:
798   http://science.sciencemag.org/content/278/5335/135.abstract

799 Peters J (2014) The role of genomic imprinting in biology and disease: An expanding view.
800   *Nat. Rev. Genet.* **15:** 517–530

801 Plagge A, Gordon E, Dean W, Boiani R, Cinti S, Peters J & Kelsey G (2004) The imprinted
802   signaling protein XLαs is required for postnatal adaptation to feeding. *Nat. Genet.* **36:**
803   818–826

804 Proudhon C, Duffié R, Ajjan S, Cowley M, Iranzo J, Carbajosa G, Saadeh H, Holland ML,
805   Oakey RJ, Rakyan VK, Schulz R & Bourc'his D (2012) Protection against De Novo
806   Methylation Is Instrumental in Maintaining Parent-of-Origin Methylation Inherited from
807   the Gametes. *Mol. Cell* **47:** 909–920

808 Quenneville S, Verde G, Corsinotti A, Kapopoulou A, Jakobsson J, Offner S, Baglivo I,
809   Pedone P V., Grimaldi G, Riccio A & Trono D (2011) In embryonic stem cells,
810   ZFP57/KAP1 recognize a methylated hexanucleotide to affect chromatin and DNA
811   methylation of imprinting control regions. *Mol. Cell* **44:** 361–372

812 Raetzman LT, Ward R & Camper S a (2002) Lhx4 and Prop1 are required for cell survival
813   and expansion of the pituitary primordia. *Development* **129:** 4229–39

814 Rizzoti K (2015) Genetic regulation of murine pituitary development. *J. Mol. Endocrinol.* **54:**
815   R55–R73

816 Robinson MD, McCarthy DJ & Smyth GK (2009) edgeR: a Bioconductor package for
817   differential expression analysis of digital gene expression data. *Bioinformatics* **26:** 139–
818   140 Available at: https://doi.org/10.1093/bioinformatics/btp616

819 Saper CB & Lowell BB (2014) The hypothalamus. *Curr. Biol.* **24:** R111–R1116

820 Savage MO (2013) Insulin-Like Growth Factors, Nutrition and Growth. In *World Review of*
821   *Nutrition and Dietetics* pp 52–59. Available at:
822   https://www.karger.com/DOI/10.1159/000342577

823 Schaller F, Watrin F, Sturny R, Massacrier A, Szepetowski P & Muscatelli F (2010) A single
824   postnatal injection of oxytocin rescues the lethal feeding behaviour in mouse newborns

825   deficient for the imprinted Magel2 gene. *Hum. Mol. Genet.* **19:** 4895–4905

826   Schulz R, Woodfine K, Menheniott TR, Bourc'his D, Bestor T & Oakey RJ (2008) Wamidex:

827   A web atlas of murine genomic imprinting and differential expression. *Epigenetics* **3:**

828   89–96

829   Seah MKY & Messerschmidt DM (2017) From Germline to Soma: Epigenetic Dynamics in

830   the Mouse Preimplantation Embryo. *Curr. Top. Dev. Biol.* **128:** 203–235

831   Stanley BG & Leibowitz SF (1984) Neuropeptide Y: stimulation of feeding and drinking by

832   injection into the paraventricular nucleus. *Life Sci.* **35:** 2635–2642

833   Swaab DF (1997) Prader-Willi syndrome and the hypothalamus. *Acta Paediatr. Suppl.* **423:**

834   50–54

835   Takahashi N, Coluccio A, Thorball CW, Planet E, Shi H, Offner S, Turelli P, Imbeault M,

836   Ferguson-Smith AC & Trono D (2019) ZNF445 is a primary regulator of genomic

837   imprinting. *Genes Dev.* **33:** 49–54 Available at:

838   https://pubmed.ncbi.nlm.nih.gov/30602440

839   Thissen J-P, Ketelslegers J-M & Underwood LE (1994) Nutritional Regulation of the Insulin-

840   Like Growth Factors*. *Endocr. Rev.* **15:** 80–101

841   Tucci V, Isles AR, Kelsey G, Ferguson-Smith AC, Tucci V, Bartolomei MS, Benvenisty N,

842   Bourc'his D, Charalambous M, Dulac C, Feil R, Glaser J, Huelsmann L, John RM,

843   McNamara GI, Moorwood K, Muscatelli F, Sasaki H, Strassmann BI, Vincenz C, et al

844   (2019) Genomic Imprinting and Physiological Processes in Mammals. *Cell* **176:** 952–

845   965

846   Voss JW & Rosenfeld MG (1992) Anterior pituitary development: Short tales from dwarf

847   mice. *Cell* **70:** 527–530

848   Wolf JB & Hager R (2006) A Maternal–Offspring Coadaptation Theory for the Evolution of

849   Genomic Imprinting. *PLOS Biol.* **4:** e380

850   Xie W, Barr CL, Kim A, Yue F, Lee AY, Eubanks J, Dempster EL & Ren B (2012) Base-

851   resolution analyses of sequence and parent-of-origin dependent DNA methylation in the

852   mouse genome. *Cell* **148:** 816–831

853

854

855   **SUPPLEMENTAL DATA**

856

857   **Generation and characterization of the *Zdbf2*-GOF line**

858   We previously reported the CRISPR/Cas9-mediated generation of *Liz*-LOF mutant mice

859   through targeting a 1.7kb deletion of the entire first exon of *Liz,* including its canonical

860   transcription start site (TSS) (Greenberg et al., 2017). Among the founder mice, some carried

861   a deletion smaller than expected, resulting from non-homologous end joining (NHEJ) repair of

862   the cut induced by the left sgRNA only. Two of these lines –CRISPR-*Liz*_379 and CRISPR-

863   *Liz*_397– exhibited a 924bp and 768bp deletion, respectively, which spanned the region

864   upstream of the *Liz* TSS and left most of the exon 1 of *Liz* intact (Figure S4D). These two lines

865   exhibited an unexpected pattern of DNA methylation at the *Zdbf2* locus upon maternal

866   transmission only: heterozygous embryos at E9.5 with a maternally inherited allele showed a

867   significant gain of sDMR DNA methylation as compared to their WT littermates (Figure S4G).

868   We further demonstrated that the sDMR remained constitutively hypermethylated in adult

869   tissues representative of the three germ layers (Figure S4E).

870   We previously demonstrated that sDMR DNA methylation is positively associated with

871   expression *in cis* of *Zdbf2* in the postnatal hypothalamo-pituitary axis (Greenberg et al., 2017).

872   To decipher if hypermethylation of the sDMR would be able to impact on *Zdbf2* expression,

873   we measured by RT-qPCR the level of *Zdbf2* mRNA in the hypothalamus and the pituitary

874   gland of 3 week-old animals. Focusing on the CRISPR-*Liz*_379 line, we showed increased

875   *Zdbf2* expression upon maternal transmission of the deletion (Figure S4F) and thus named

876   this mutant as *Zdbf2*-gain-of-function (*Zdbf2*-GOF). Allelic analysis from hybrid mice between

877   C57Bl6/J and JF1 strains demonstrated that this gain-of-function was due to ectopic DNA

878   methylation at the sDMR on the maternal allele and ectopic expression of the normally silent

879   maternal *Zdbf2* allele (Figure 3A and B). Reactivation of the maternal allele resulted in bi-

880   allelic, rather than strictly paternal mono-allelic expression of *Zdbf2*. The level of expression of

881   the maternal allele was not equal to the expression of the paternal allele, resulting in a net 1.7-

882   fold increase of *Zdbf2* in *Liz*-GOF animals compared to WT levels (Figure S4F). This was

883   linked to a mosaic gain of DNA methylation on the maternal allele of *Zdbf2*-GOF animals, with

884   70% versus 90-95% of paternal methylation levels. Allelic analysis revealed cellular

885   heterogeneity in the acquisition of methylation of the maternal allele (Figure S4H). In contrast

886   to the effect of the maternal allele, paternal transmission of the deletion behaved as a silent

887   mutation (Figure S4E and F).

888   In sum, we have generated mutant mice with loss-of-imprinting of the *Zdbf2* locus,

889   harboring increased *Zdbf2* dosage in the postnatal brain, as a result of abnormal biallelic

890   expression. The deletion had no effect on the sex and Mendelian distributions upon both

34

891   maternal and paternal transmission (Figure S5A and B) and the mice survived at the same

892   rate as their WT littermates (Figure S5C). Moreover, we did not detect any fertility or behavioral

893   phenotype in the *Zdbf2*-GOF mice.
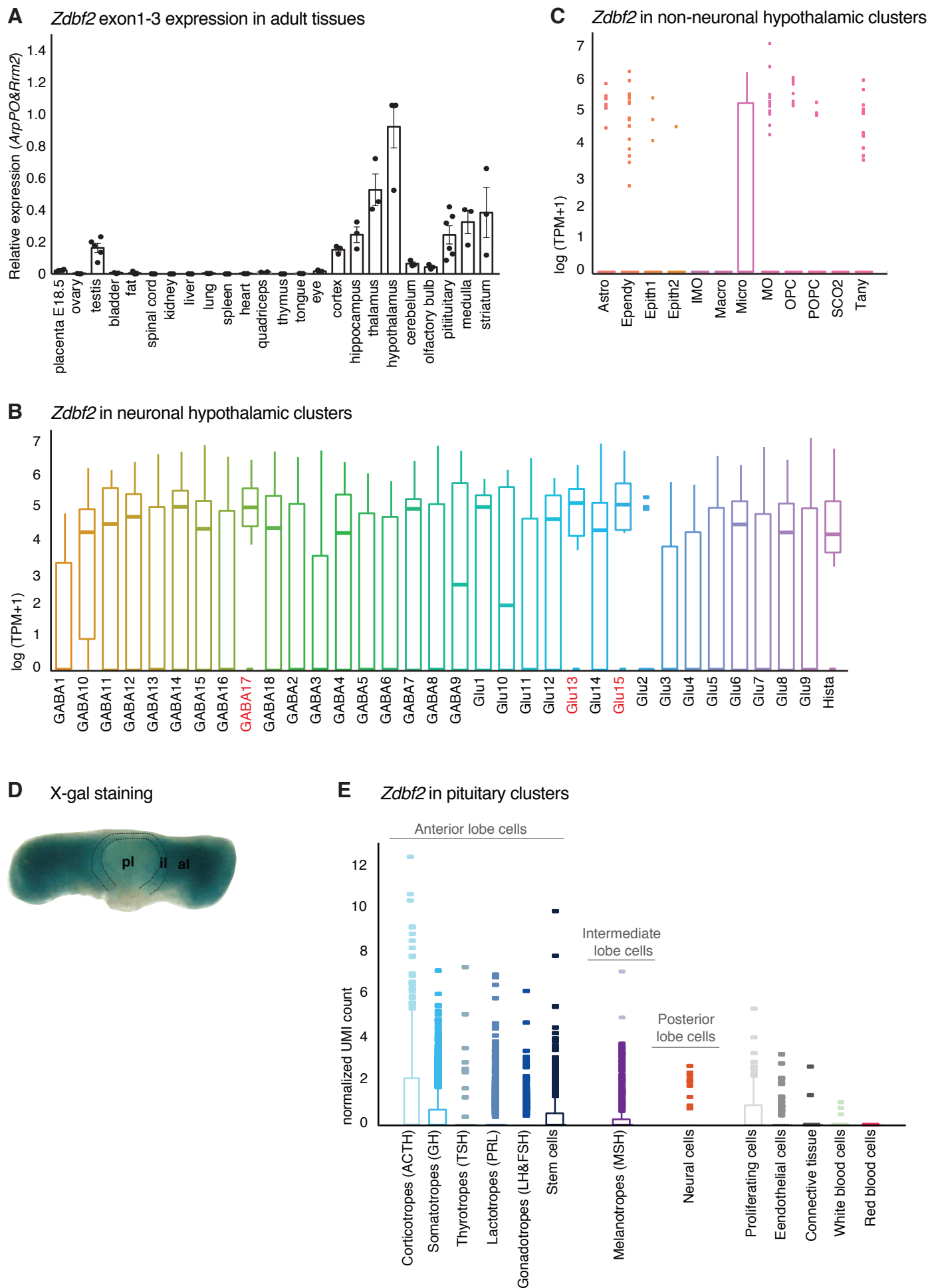
Glaser et al._ Supplemental Figure 1

A *Zdbf2* exon1-3 expression in adult tissues

C *Zdbf2* in non-neuronal hypothalamic clusters

B *Zdbf2* in neuronal hypothalamic clusters

D X-gal staining

E *Zdbf2* in pituitary clusters

Figure S1: *Zdbf2* **expression from pituitary and hypothalamus.**
(**A**) Expression of *Zdbf2* measured by RT-qPCR in a bank of adult (6-weeks old) mouse tissues. *Zdbf2* is preferentially expressed in the brain and hypothalamus is the tissue showing the highest level of expression. Data are shown as means ± s.e.m. This figure has been adapted from Greenberg et *al* 2017. (**B, C**) Expression of *Zdbf2* in hypothalamic neuronal (**B**) and non-neuronal (**C**) cell clusters. Clusters where *Zdbf2* expression is the highest are highlighted in red. Single-cell RNA-seq datasets from the hypothalamus of 8 to 10 week-old B6D2F1 females from Chen *et al.*, Cell Reports, 2017. (**D**) Whole-mount pituitary from a *Zdbf2*-LacZ KI mouse stained with X-gal. pl, posterior lobe; il, intermediate lobe; al, anterior lobe. (**E**) Expression of *Zdbf2* in pituitary cell clusters. *Zdbf2* expression is found predominantly in cluster of cells from the anterior and intermediate lobes. Single-cell RNA-seq datasets from pituitaries of 7 week-old C57BL/6J males from Cheung *et al.*, Endocrinology, 2018.
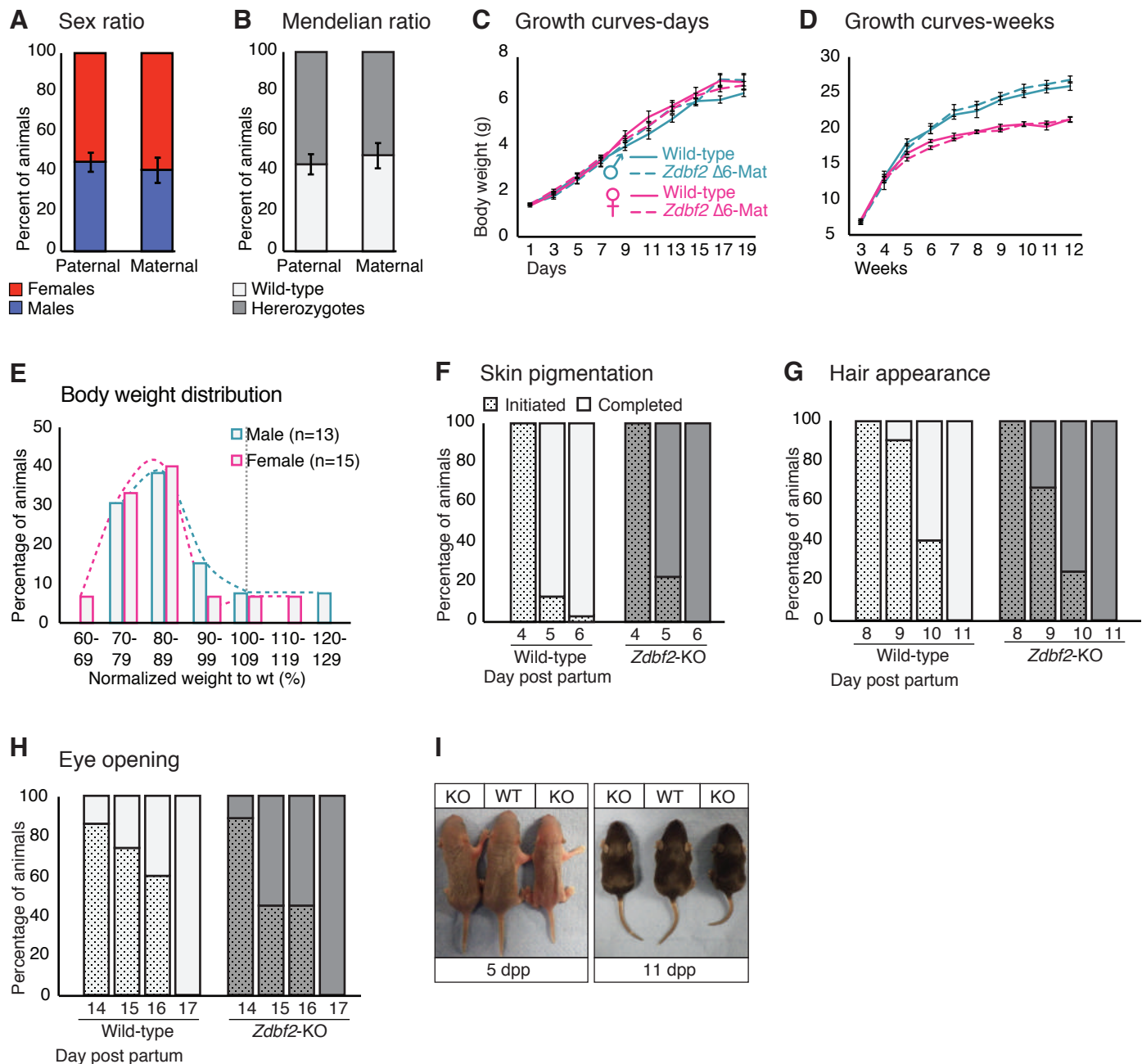
Glaser et al._ Supplemental Figure 2

Figure S2: *Zdbf2*-KO pups acquire normal hallmarks of postnatal development.
(**A, B**) Sex ratio (**A**) and genotype ratio (**B**) observed at birth (1dpp) among *Zdbf2* heterozygotes from paternal and maternal transmission of the deletion after three backcrosses. Data are shown as means ± s.e.m. from individuals from n= 32 and 12 litters from paternal and maternal transmission respectively. (**C, D**) Growth curves as in Figure 2C and Figure 2D, respectively, but comparing mutants with a maternal transmission of the Zdbf2 deletion with their WT litter-mates. (**E**) Frequency of body weight distribution for normalized weights of 2 week-old *Zdbf2*-KO mice relative to WT mice (100%) grouped into 10% bins. The weight reduction phenotype appears to be highly penetrant. (**F-H**) Graphical representation of the timing of three typical hallmarks of postnatal development: skin pigmentation (**F**), hair appearance (**G**) and eye opening (**H**) between WT and *Zdbf2*-KO littermates. (**I**) Representative photography of WT and *Zdbf2*-KO female littermates at 5dpp (left) and 11dpp (right).
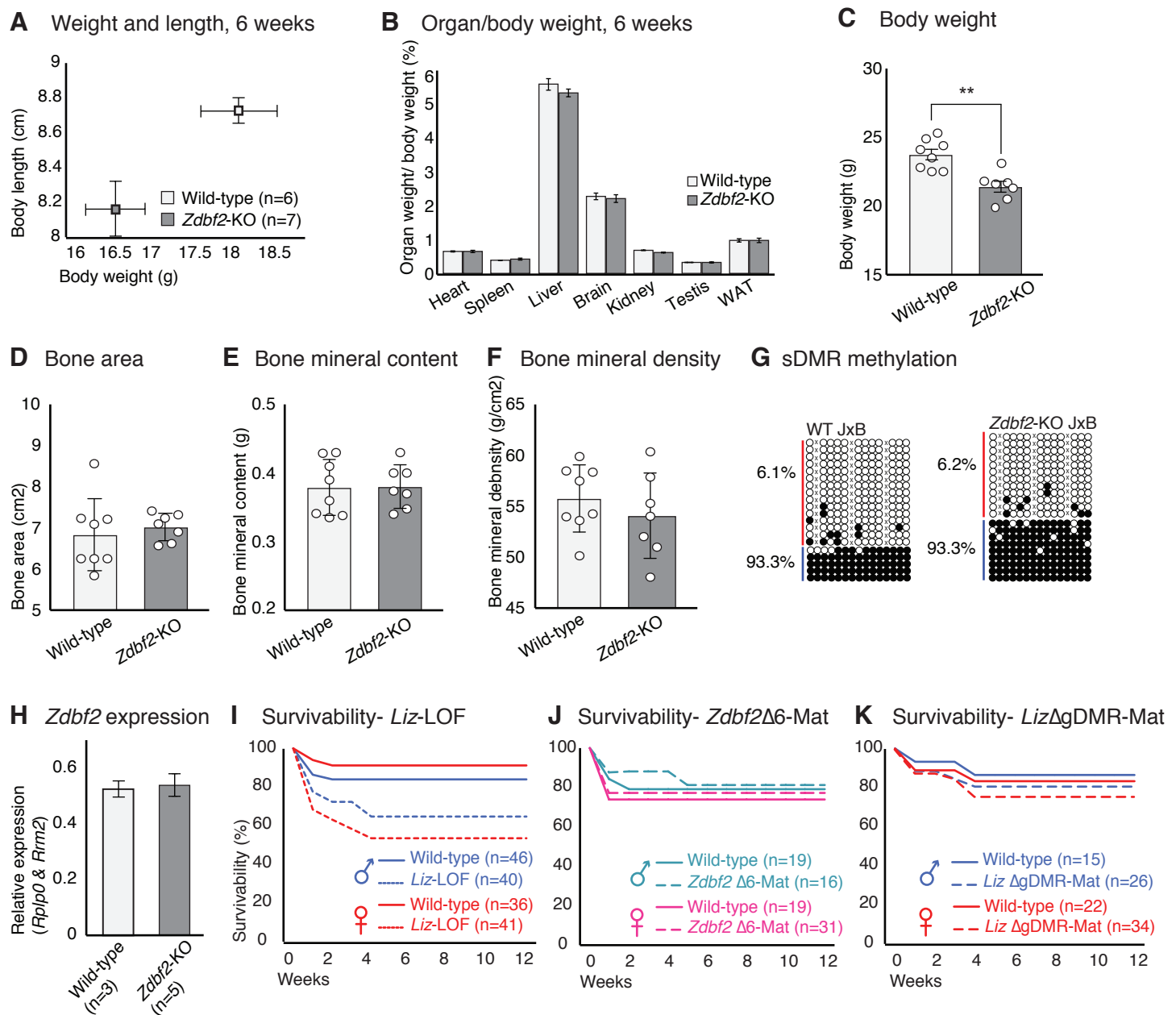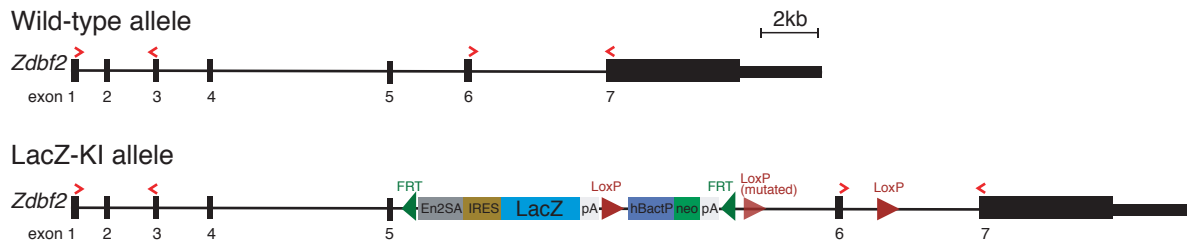
Glaser et al._ Supplemental Figure 3

Figure S3: Phenotypic and molecular characterization of *Zdbf2* mutants.
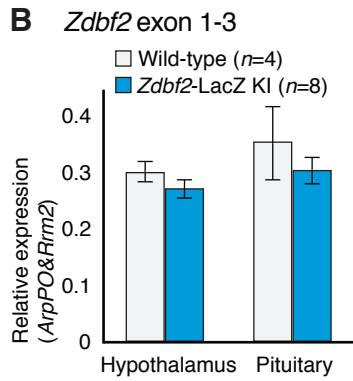(**A**) Average body length and weight of n WT and *Zdbf2*-KO mice at 6 weeks. (**B**) Individual organ weight plotted as percentage of total body weight in *Zdbf2*-KO mice and WT littermates at 6 weeks.
(**C-F**) Dual-energy X-ray absorptiometry (DXA) showing calculation of body weight (**C**), bone area (**D**), bone mineral content (**E**) and bone mineral density (**F**). Data are shown as means s.e.m from n=8 WT and 7 *Zdbf2*-KO males. (**G**) Bisulfite cloning and sequencing of the sDMR from hypothalamus DNA of 3 week-old hybrid WT (top) and *Zdbf2*-KO (bottom) mice (JF1 x *Zdbf2*-KO cross) reveals that the deposition of DNA methylation at the sDMR is not affected by *Zdbf2* deletion. Red, maternal alleles; blue, paternal alleles. cross, informative JF1 SNP. (**H**) RT-qPCR measuring *Zdbf2* expression from exon 1 to 3 in 3 week-old hypothalamus reveals that *Zdbf2* transcriptional output is not affected by the deletion of the exon 6. Statistical analyses were performed by a two-tailed, unpaired, nonparametric Mann Whitney t test. **p<0.01. (**I-K**) Kaplan-Meier curves of the survivability as in Figure 2I but comparing WT and *Liz*-LOF males and females (**I**), WT and *Zdbf2*-Δexon6 males and females upon maternal transmission of the deletion (**J**) and WT and *Liz*-Δ gDMR males and females upon maternal transmission of the deletion (**K**).
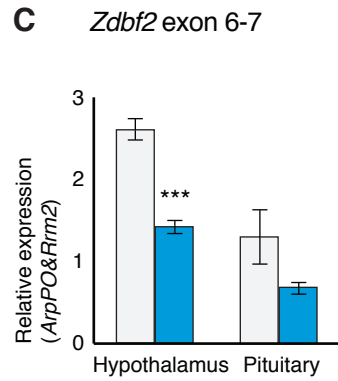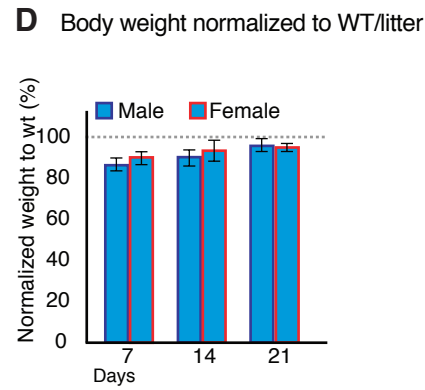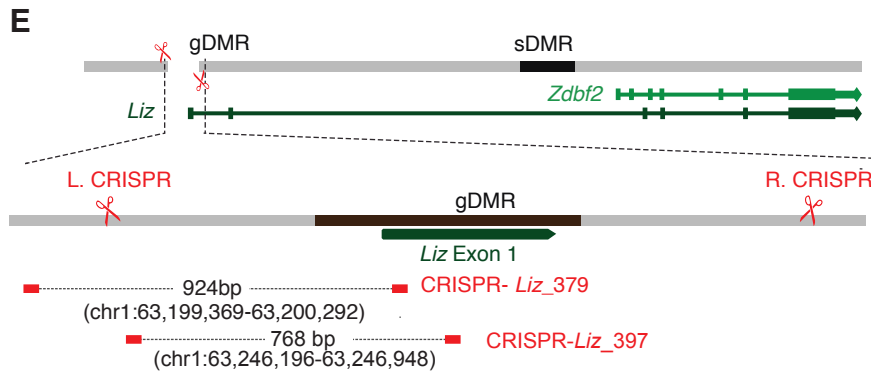
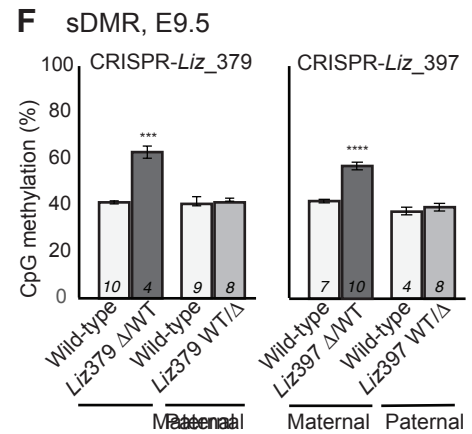Glaser et al._ Supplemental Figure 4

A

Wild-type allele

B *Zdbf2* exon 1-3

C *Zdbf2* exon 6-7

D Body weight normalized to WT/litter

E

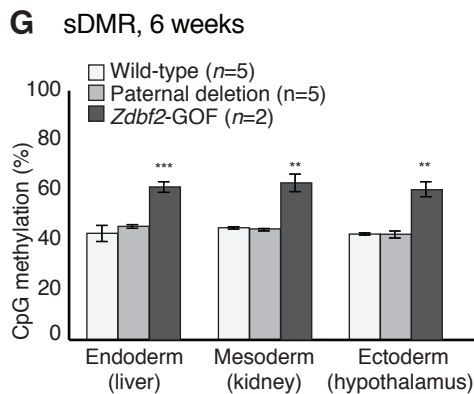**F** sDMR, E9.5

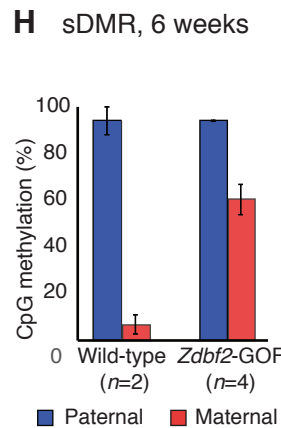**G** sDMR, 6 weeks

H sDMR, 6 weeks

Figure S4: Characterization of partial *Zdbf2*-LOF and *Zdbf2*-GOF mouse lines.
(**A**) Scheme of the wild-type and LacZ-KI *Zdbf2* alleles. The seven exons of the *Zdbf2* transcript are represented by black boxes and the primers used for the RT-qPCR in (**B,C**) are labeled as red arrows. The LacZ-KI allele contains an insertion of: a trapping cassette (En2SA-IRES-LacZ-pA), a Neo cassette under the human beta actin promoter (hbactP-Neo-pA) together with FRT sites to delete the cassettes and LoxP sites to delete exon 6. However, we found the middle loxP site to be non-functional because of a point mutation in the original EUCOMM-provided ES cells. (**B, C**) *Zdbf2* expression measured by RT-qPCR from exon 1-3 (**B**) and exon 6-7 (**C**) in hypothalamus and pituitary of WT and *Zdbf2*-LacZ KI individuals. The insertion schematized in (**A**) leads to a ~ 2-fold decrease in *Zdbf2* expression at exon 6-7, probably due to exon skipping. Data are shown as means ± s.e.m. from n individuals. Statistical analyses were performed by a two-tailed, unpaired, nonparametric Mann Whitney t test. ***$p<0.001$. (**D**) Normalized body growth of *Zdbf2*-LacZ KI mice to their WT littermates (100%) followed at 1, 2 and 3 weeks shows a slight decrease in weight of both males and females. Data are shown as means ± s.e.m. from 8 litters. (**E**) Graphic model of the ΔgDMR CRISPR deletion leading to the generation of the *Liz*_379 founder line (*Zdbf2*-GOF). Deletion is the results of a single cut by Cas9 at the left sgRNA position, followed by NHEJ. (**F**) Bisulfite-pyrosequencing from post-implantation embryos at E9.5 shows increase of sDMR CpG methylation only upon maternal transmission of the deletion, both in *Liz*_379 (left) and *Liz*_397 (right) CRISPR lines. (**G**) Bisulfite-pyrosequencing shows increased sDMR methylation in tissues from 6 week-old mice when the deletion is maternally transmitted. The paternal transmission of the deletion behaves as silent. (**H**) Quantification of allelic sDMR CpG methylation measured by bisulfite cloning and sequencing from n WT and *Zdbf2*-GOF adult tissues. The gain of sDMR methylation from the maternal allele in the mutant compared to their WT littermates is about 65%.
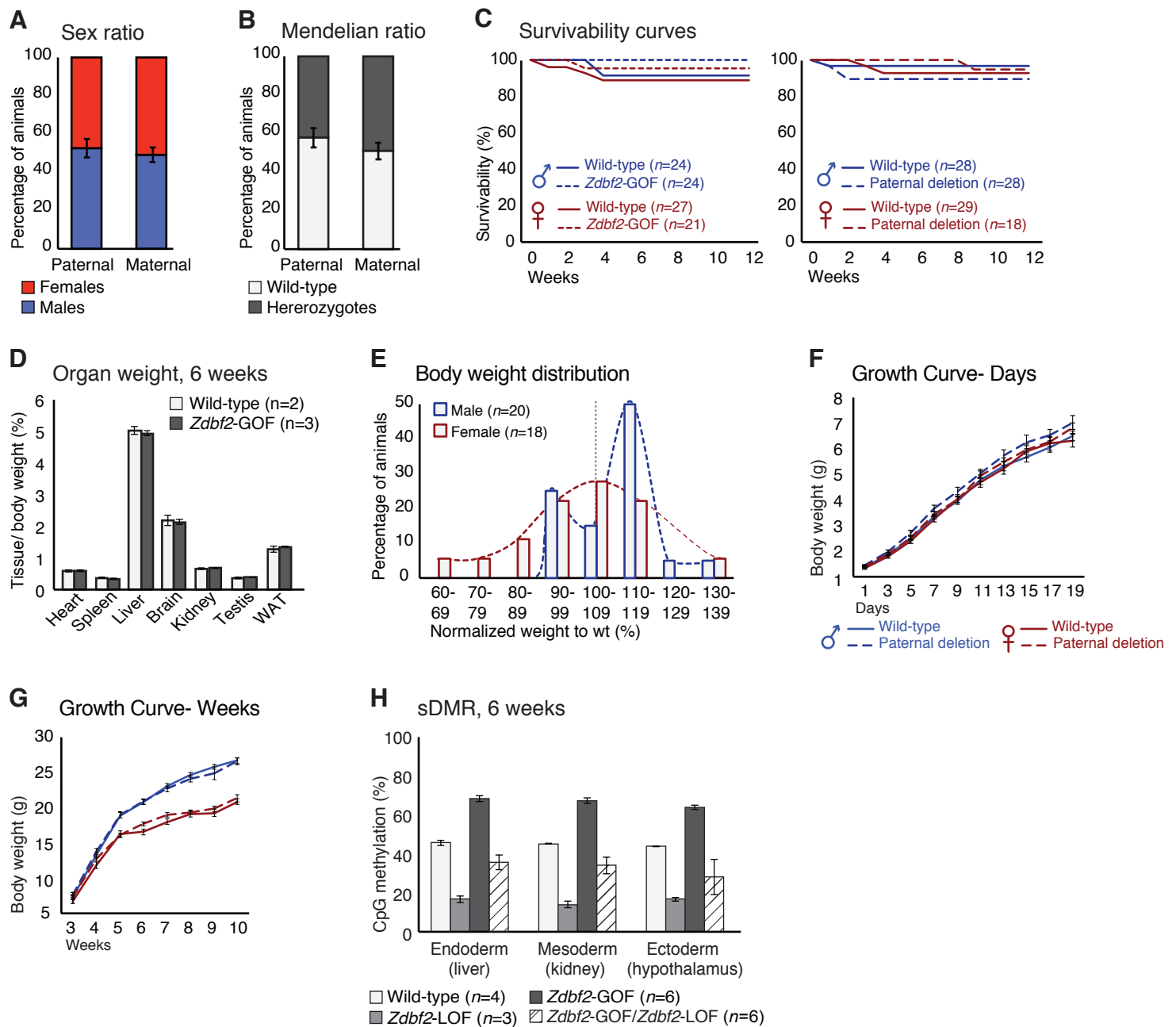
Glaser et al._ Supplemental Figure 5

Figure S5: Phenotypic characterization of *Zdbf2*-GOF mutants.
(**A, B**) Sex ratio (**A**) and genotype ratio (**B**) observed at birth among heterozygotes upon paternal and maternal transmission of the *Zdbf2*-GOF mutation after three backcrosses of the *Liz*_379 line. Data are shown as means ± s.e.m. from individuals from n= 15 and 20 litters from paternal and maternal transmission respectively. (**C**) Kaplan-Meier curves of the survivability from birth to 12 weeks showing no lethality phenotype upon maternal (left) and paternal (right) transmission of the deletion, both in males and females. Data are shown as means ± s.e.m. from n individuals. (**D**) Individual organ weight plotted as percentage of total body weight in *Zdbf2*-GOF mice and WT littermates at 6 weeks. (**E**) Frequency of weight distribution for normalized weights of 2-week-old *Zdbf2*-GOF mice relative to WT mice (100%) grouped into 10% bins. The male specific overgrowth phenotype appears to be penetrant. Females show a normal distribution of weight, confirming the sex-specific phenotype seen in C and D. (**F, G**) Growth curves as in Figure 5D and 5E, but comparing the mutants with a paternal transmission of the deletion with their WT littermates. The paternal deletion behaves as a silent mutation with no growth-related phenotype in the progenies. n=10–25 mice were analyzed per genotype, depending on age and sex. (**H**) Bisulfite-pyrosequencing shows an almost complete rescue of the *Zdbf2*-LOF defects of sDMR methylation in tissues of *Zdbf2*-GOF /*Zdbf2*-LOF mice at 6 weeks. Data are shown as means ± s.e.m. from n individuals. Statistical analyses were performed by a two-tailed, unpaired, nonparametric Mann Whitney t test. *p ≤ 0.05
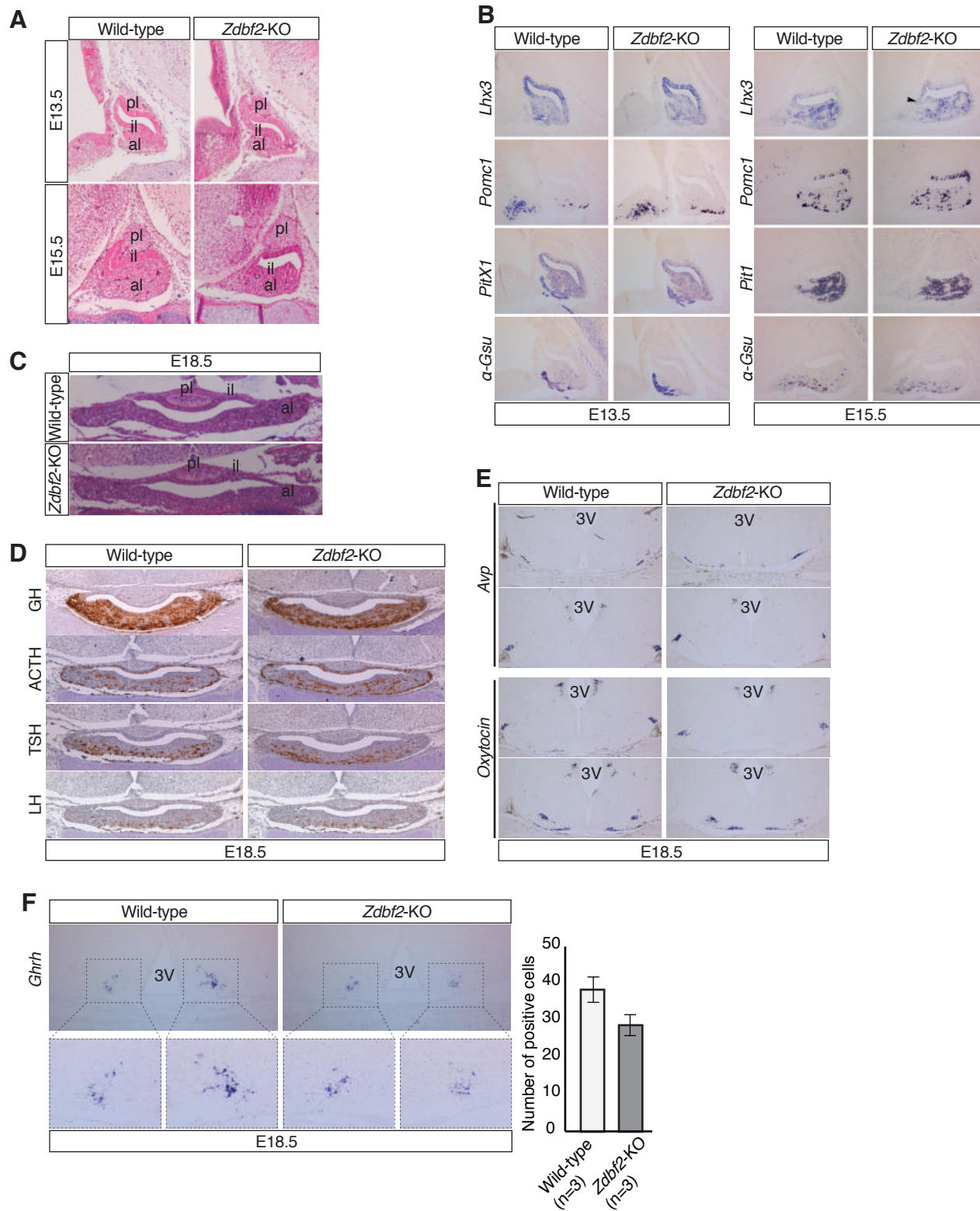
Glaser et al._ Supplemental Figure 6

Figure S6: Normal development of the hypothalamo-pituitary axis in *Zdbf2*-KO mice.
(**A**) Haematoxylin-Eosin (H&E) staining reveals normal development of the pituitary at embryonic day (E) 13.5 and E15.5 embryonic days. (**B**) RNA in situ hybridization for pituitary lineage-specific genes reveals normal mRNA expression of cell specification markers in the pituitary of the *Zdbf2*-KO embryos at E13.5 and E15.5. (**C**) Morphological assessment of the mature E18.5 pituitary gland by H&E staining shows no phenotype in the pituitary gland before birth. (**D**) Immunohistochemistry analysis of four pituitary hormones (GH, ACTH, TSL, LH) at E18.5 suggests no obvious defect in hormone-producing cells in the anterior lobe of the pituitary before birth. (**E**) In situ hybridization for two hypothalamic neuropeptides, arginine vasopressin (AVP) (top) and oxytocin (bottom), in the developing E18.5 hypothalamus suggests no apparent differences in AVP and oxytocin transcripts. (**F**) RNA in situ hybridization for *Ghrh* on E18.5 hypothalamus shows trend towards decreased expression of *Ghrh* in mutant embryos compared to controls, although difference is not statistical significant. Quantification (right panel) represents the means ± s.e.m of the number of *Ghrh* positive cells over n=3 independent experiments. Overall, results in **A-F** are congruent with the observation of normal weight distribution in *Zdbf2*-KO E18.5 embryos (Figure 2B). pl, posterior lobe; il, intermediate lobe; al, anterior lobe; 3V, third ventricle of the hypothalamus.

Glaser et al._ Supplemental Figure 7
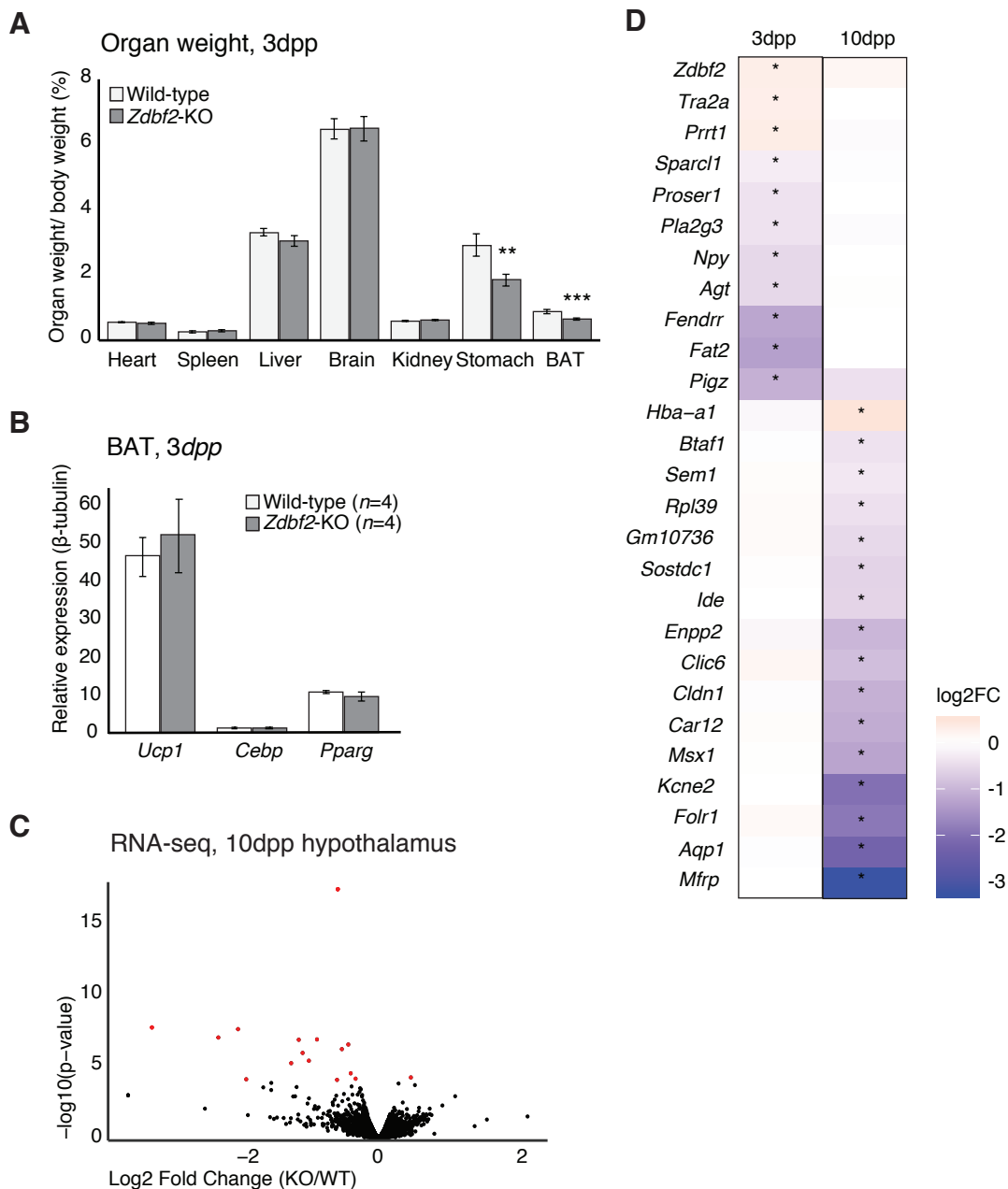
Figure S7: Characterization of the early postnatal feeding behavior in *Zdbf2*-KO pups.
(**A**) Individual organ weight plotted as percentage of total body weight in *Zdbf2*-KO mice and WT littermates at 3dpp. (**B**) RT-qPCR from BAT measuring the mRNAs level of three markers of BAT activity (*Ucp-1*, *Cebp* and *Pparg*) between WT and *Zdbf2*-KO at 3dpp. (**C**) Volcano plot representation of RNA-seq of 10dpp hypothalamus of *Zdbf2*-KO versus WT littermates. Red dots: differentially expressed genes with a threshold of FDR<10%. (**D**) Heatmap showing the log2 fold change of expression of the differentially expressed genes (DEGs) in the hypothalamus of *Zdbf2*-KO pups at 3 and 10dpp. There is no overlap between the DEGs at 3 and 10dpp. Stars represent significant change of expression (FDR<10%).

Supplemental Table 1: Survivability counts from different transmission of the *Zdbf2*-KO allele.

A. *Zdbf2*-KO (paternal transmissiom)		1	3	5	7	9	11	13	15	17	19	21	28	35	42	49	56	63	70	77	84
Days post partum		1	3	5	7	9	11	13	15	17	19	21	28	35	42	49	56	63	70	77	84
	Males WT	44	37	37	37	37	37	37	37	37	36	36	36	36	36	36	36	36	36	36	36
n=24 litters	Female WT	50	44	44	44	44	44	44	44	43	43	40	39	39	39	39	39	39	39	39	39
	Males KO	30	17	17	17	17	16	16	16	16	16	16	16	16	16	16	16	16	16	16	16
	Female KO	57	30	30	30	30	29	29	29	28	28	28	28	28	28	28	28	27	27	27	27

B. *Zdbf2*-KO (homozygote transmissiom)		1	2	3	4	5	6	7	8	9	10	11	12	13	14	15	16	17	18	19	20	21
Days post partum		1	2	3	4	5	6	7	8	9	10	11	12	13	14	15	16	17	18	19	20	21
n=19 litters	Males KO	71	54	54	54	54	54	54	54	54	54	54	53	53	53	53	53	53	53	53	52	52
	Female KO	80	62	58	58	58	58	58	58	58	58	58	58	58	58	58	58	58	58	58	57	57

C. *Zdbf2*-Δexon6 (maternal transmissiom)		1	7	14	21	28	35	42	49	56	63	70	77	84
Days post partum		1	7	14	21	28	35	42	49	56	63	70	77	84
	Males WT	19	16	15	15	15	15	15	15	15	15	15	15	15
n=11 litters	Female WT	19	14	14	14	14	14	14	14	14	14	14	14	14
	Males KO	16	14	14	14	14	13	13	13	13	13	13	13	13
	Female KO	31	24	24	24	24	24	24	24	24	24	24	24	24

<u>Supplemental Table 1</u>: Survivability counts from different transmission of the *Zdbf2*-KO allele.

(A) Number of living pups followed every two days from 1 to 21dpp and every week from 21 to 84dpp from 24 litters coming from [female WT x male *Zdbf2* KO/WT] crosses (paternal transmission). These 24 litters come from 4 different crosses including 8 females and 4 males. Day 1 corresponds to the day of birth (1dpp). We can observe that the number of living *Zdbf2*-KO (males and females) starts decreasing from 3dpp onwards.

(B) Number of living pups followed every day from 1 to 21dpp from 19 litters coming from [female WT x male *Zdbf2* KO/KO] crosses (homozygote transmission). These 19 litters come from 5 different crosses including 10 females and 5 males. All pups from these crosses inherited a mutated allele from their dad and are thus *Zdbf2*-KO.

(C) Number of living pups followed every week from 1 to 84dpp from 11 litters coming from [female *Zdbf2* KO/WT x male WT] crosses (maternal transmission, silent mutation). These 11 litters come from 2 different crosses including 4 females and 2 males. We did not observe any survivability bias within those litters.

Supplemental Table 2: List of primers used in this study.

RT-qPCR primer

Zdbf2 exons 1-3	Fwd	CCGGAAGGAGAGCAGGAG
	Rev	GAGCAGAAAAGAGCAAGCA
Zdbf2 exons 6-7	Fwd	CTGCGACACCACCCATATAA
	Rev	AAAACCACCACCACTTCAGG
Rplp0	Fwd	TCCAGAGGCACCATTGAAATT
	Rev	TCGCTGGCTCCCACCTT
Rrm2	Fwd	CCGAGCTGGAAAGTAAAGCG
	Rev	ATGGGAAAGACAACGAAGCG
Gh exons 4-5	Fwd	CTTGAGGATCTGCCCAACAC
	Rev	CCTCGGACCGTGTCTATGAG
Igf-1 exons 2-3	Fwd	TGGATGCTCTTCAGTTCGTG
	Rev	CACTCATCCACAATGCCTGT
18S	Fwd	GCCCTGTAATTGGAATGAGTCCACTT
	Rev	GTCCCCAAGATCCAACTACGAGCTTT
ßActin	Fwd	AAGTGACGTTGACATCCG
	Rev	GATCCACATCTGCTGGAAGG

RT-pyrosequencing

Zdbf2 exon 6	Fwd	[Biotin]-GGAAATGAAGAGCAGCCCAGTAG
	Rev	GCCACTGTCTCAAGAGAACCATCA
	Seq	AACCATCACGTTCAGG

Bisulfite + Pyrosequencing Primers

sDMR	Fwd	AGATGGAAGGAAAGAATTGAATTTTATA
	Rev	[Biotin]-TACCAACCCACTATATACATTCTTCATTA
	Seq	TGAATTTTATATATTATTTTTTGAT

Bisulfite + Cloning/Sequencing Primers

sDMR	Outer Fwd	ATTTTATGTATTTATTAGTGAGTTG
	Outer Rev	CTAATCACAACTCCCAATCAC
	Inner Fwd	GAATTGAATTTTATATATTATTTTTTG
	Inner Rev	CCTATATACAACTTACCTTACTT

Genotyping Primers

Zdbf2-KO	Fwd	AGCACATTTTCTTCCATTTACTTGT
	Rev	ACTCCAGTACCCCACACACA
Zdbf2-GOF	Fwd	CACCGATTGCTAGAACTACAATGG
	Rev	GAAAGCAATGCACACACTGG
Liz-LOF	Fwd	TTTTTCTTTTGCCTCCAAGAA
	Rev	CCTGGACAGCATTTCTTTCTC
	Rev	TGGCTTTAAAACAGGGGATG

CRISPR sgRNA oligos

Zdbf2-KO	Left	CACCGCATTACAATGTATGCTACGA
		AAACTCGTAGCATACATTGTAATGC
	Right	CACCGTTTACCATGGATGCACTCCC
		AAACGGGAGTGCATCCATGGTAAAC